Electronic Supplementary Material (ESI) for Journal of Materials Chemistry A.

A general post-synthetic modification approach of amino-tagged metal-organic frameworks to access efficient catalysts for the Knoevenagel condensation reaction

Yi Luan, Yue Qi, Hongyi Gao, RADOELIZO S. Andriamitantsoa, Nannan Zheng and Ge Wang*

Beijing Key Laboratory of Function Materials for Molecule & Structure Construction, School of Materials Science and Engineering, University of Science and Technology Beijing, Beijing 100083, People's Republic of China

General Information.

Characterization.

The phase composition of the samples was investigated by X-ray powder diffraction (XRD, M21X, Cu Kα radiation, λ=0.154178 nm). The morphology and structure of the as-obtained product were characterized by scanning electron microscopy (SEM, ZEISS SUPRA55). Thermogravimetric analysis (TG) was conducted by Netzsch STA449F at a heating rate of 10 ^{o}C/min under the N_2 flow. The specific surface areas were calculated by nitrogen sorption-desorption isotherms using a Micromeritics ASAP 2420 adsorption analyzer. The pore size distributions were derived from the adsorption branches of isotherms by using the Barrett-Joyner-Halenda (BJH) model. Fourier transform infrared spectroscopy (FTIR) was acquired on Nicolet 6700 using the KBr pellet technique. The results were analyzed by gas chromatography-mass spectrometry using an internal standard (GC-MS, Agilent7890/5975C-GC/MSD, HP5-MS column, Ar carrier gas, 200 ºC). Infrared spectra were recorded on a Nicolet Nexus 670 FT-IR ESP spectrophotometer. Analytical thin layer chromatography was performed using EMD 0.25 mm silica gel 60-F plates.

General procedure for Knoevenagel condensation reaction of aldehyde and malononitrile

In a typical reaction, to a 5 mL reaction vessel was added 1.0 mmol benzaldehyde and 1.5 mmol malononitrile in 2 mL of toluene. To the reaction was then added 1.0 mol% of catalyst. The heterogeneous solution was stirred at room temperature (23 ºC) for 2 h. The final yield and selectivity of the Knoevenagel condensation product was analyzed by GC-MS using *n*-dodecane as the internal standard.

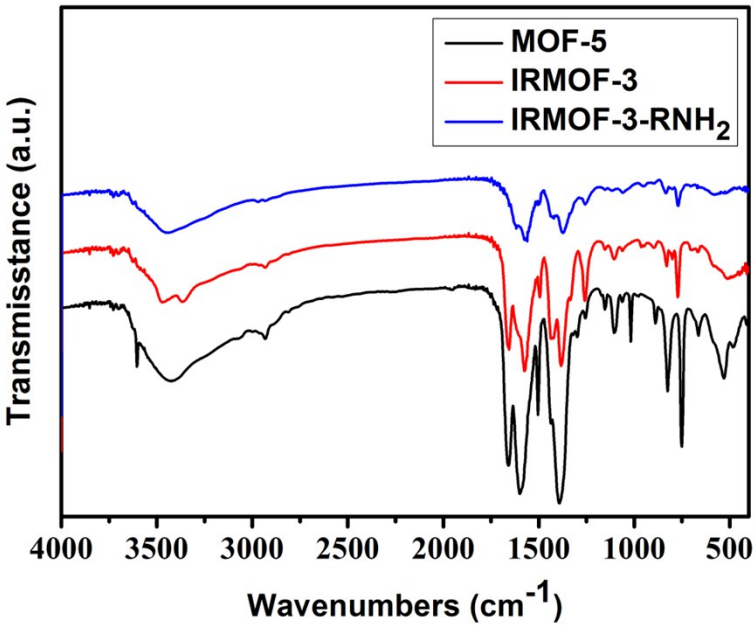

Figure S1. FTIR of MOF5, IRMOF-3 and IRMOF-3-RNH_2

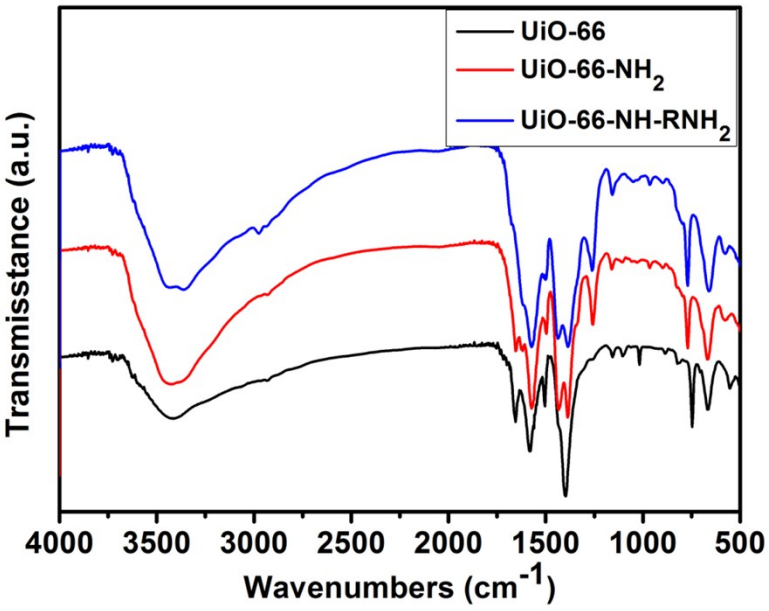

Figure S2. FTIR of UiO-66, UiO-66-NH_2 and UiO-66-NH-RNH_2

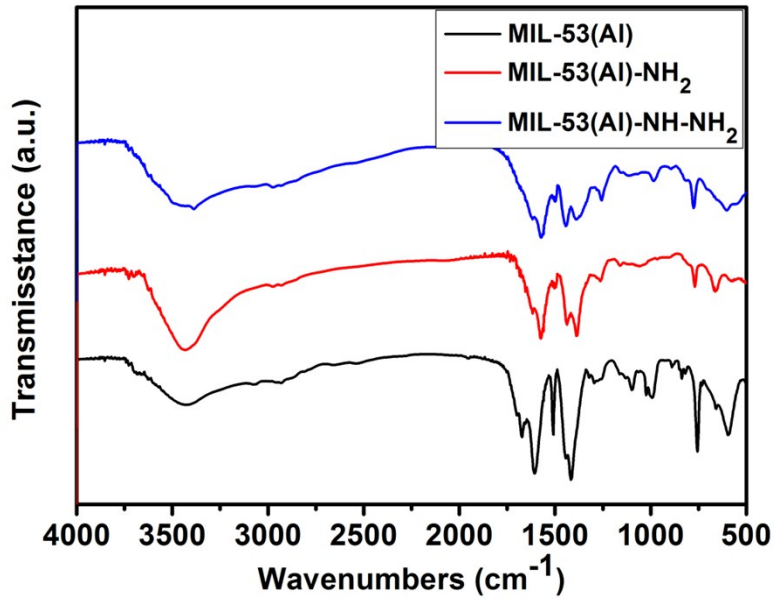

Figure S3. Al-53, Al-MIL-53-NH_2 and Al-MIL-53-NH-RNH_2

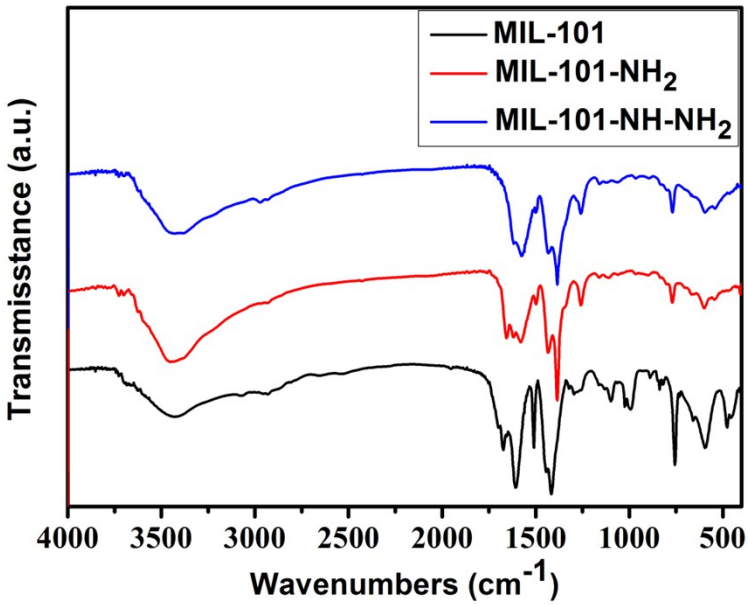

Figure S4. Cr-MIL-101, Cr-MIL-101-NH_2 and Cr-MIL-101-NH-RNH_2

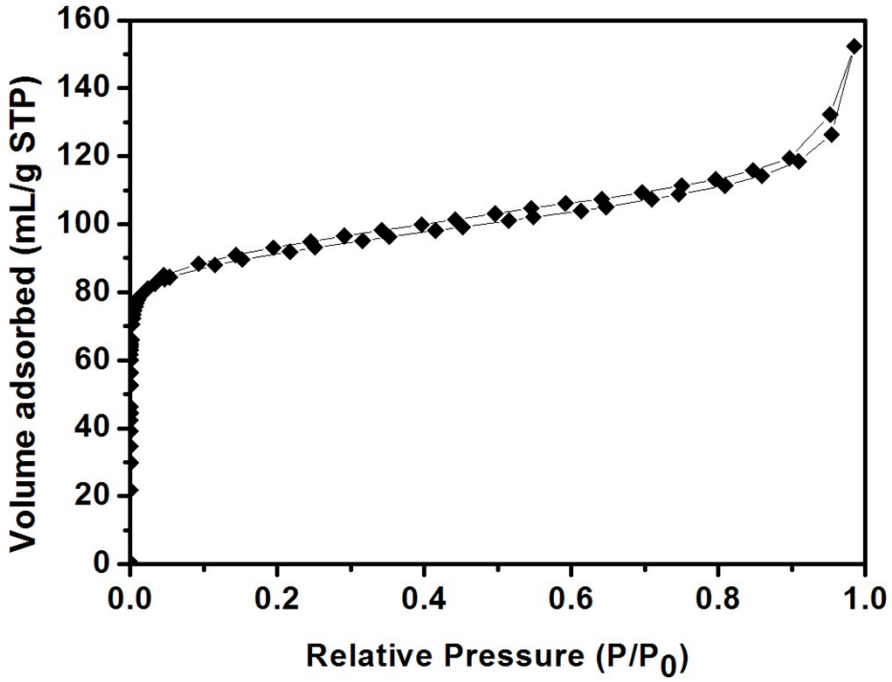

Figure S5. Nitrogen adsorption/desorption isotherms of IRMOF-3

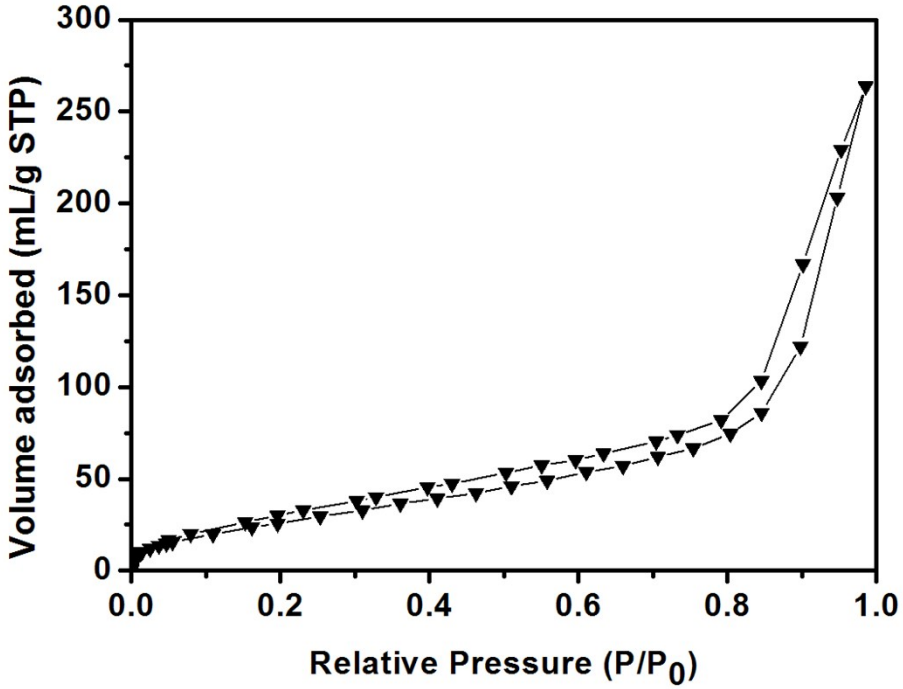

Figure S6. Nitrogen adsorption/desorption isotherms of IRMOF-3-RNH_2

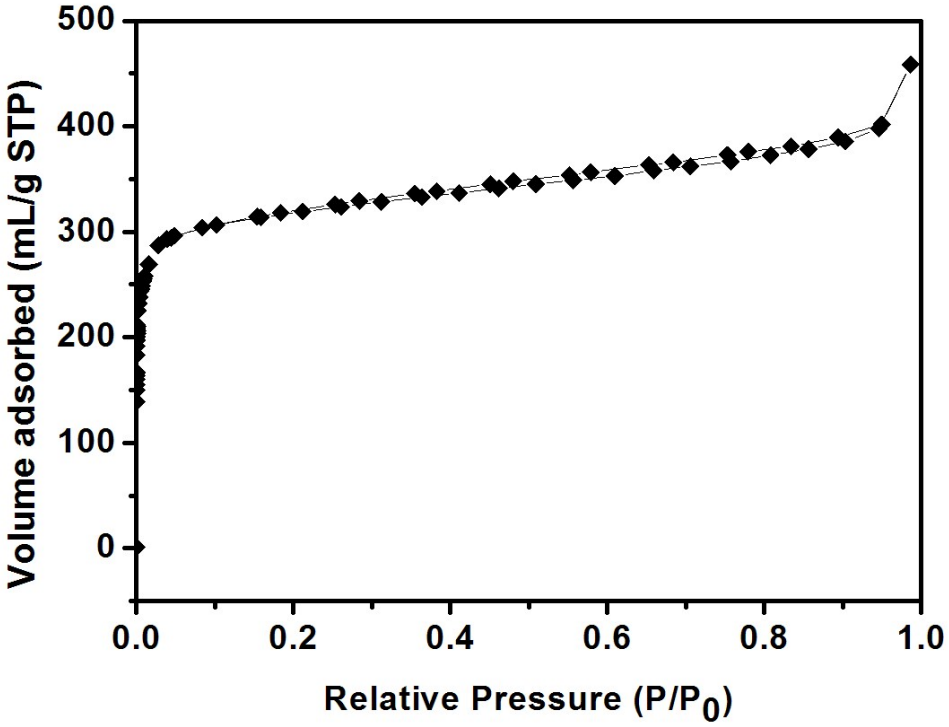

Figure S7. Nitrogen adsorption/desorption isotherms of UiO-66-NH_2

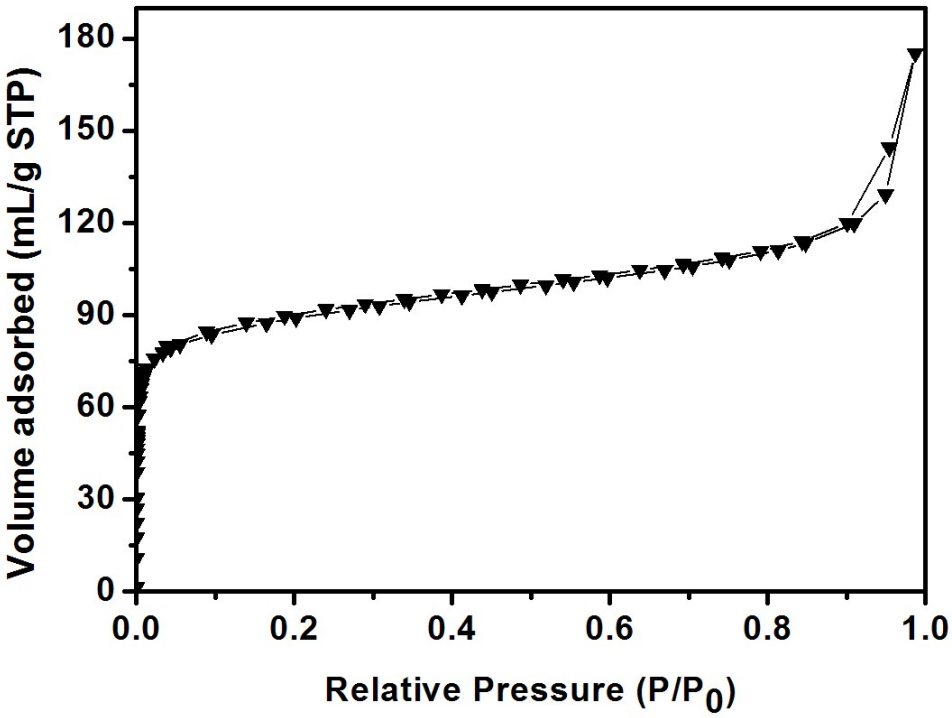

Figure S8. Nitrogen adsorption/desorption isotherms of UiO-66-NH-RNH_2

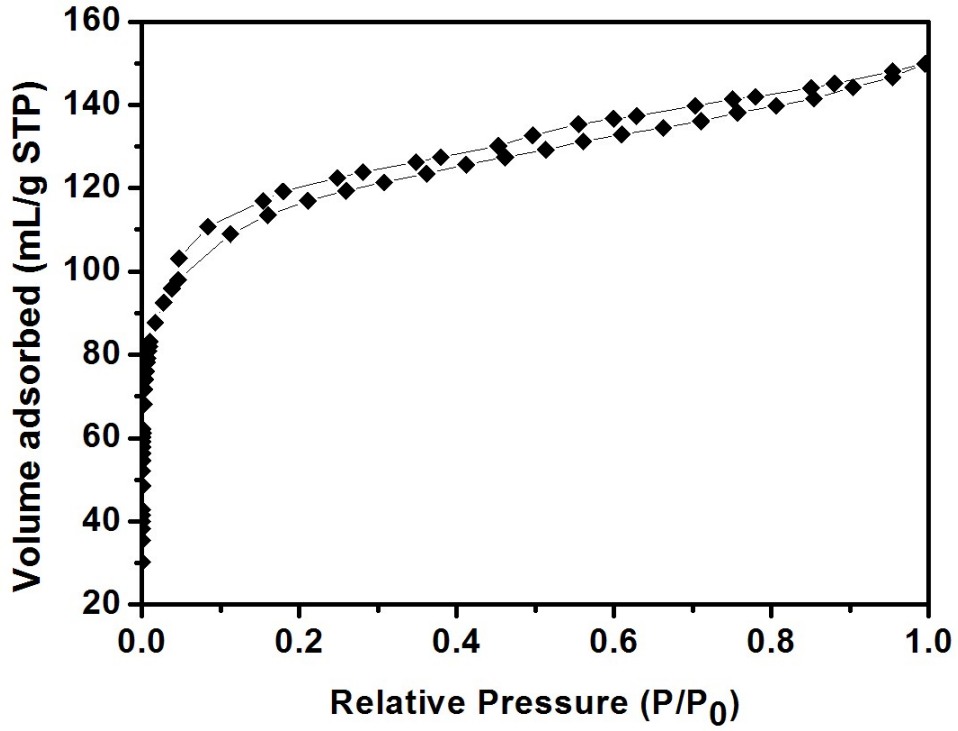

Figure S9. Nitrogen adsorption/desorption isotherms of Al-MIL-53-NH_2

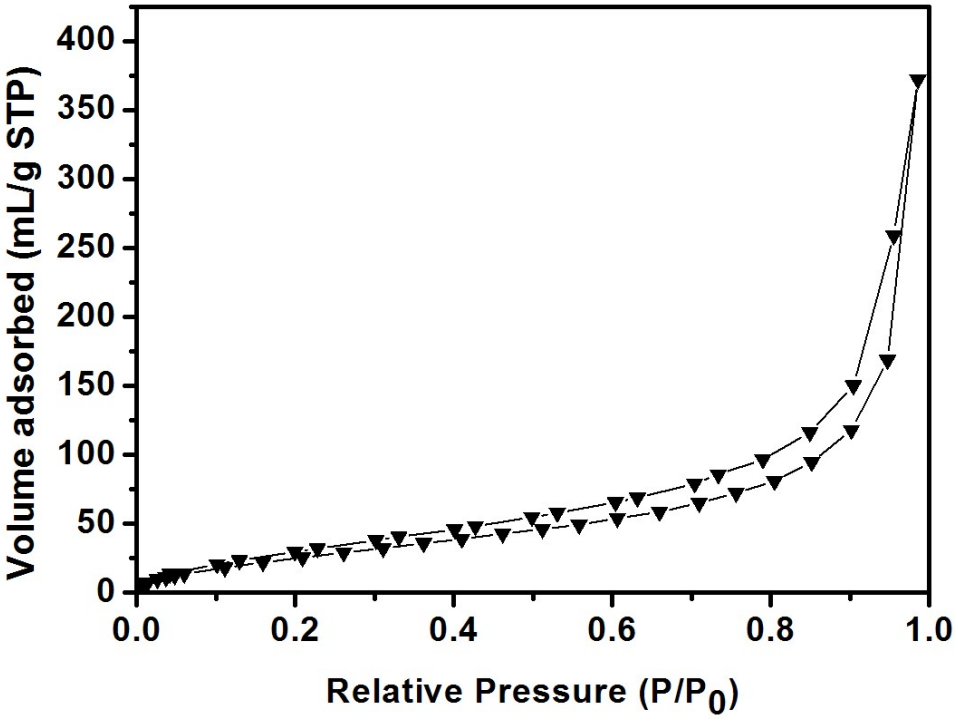

Figure S10. Nitrogen adsorption/desorption isotherms of Al-MIL-53-NH-RNH_2

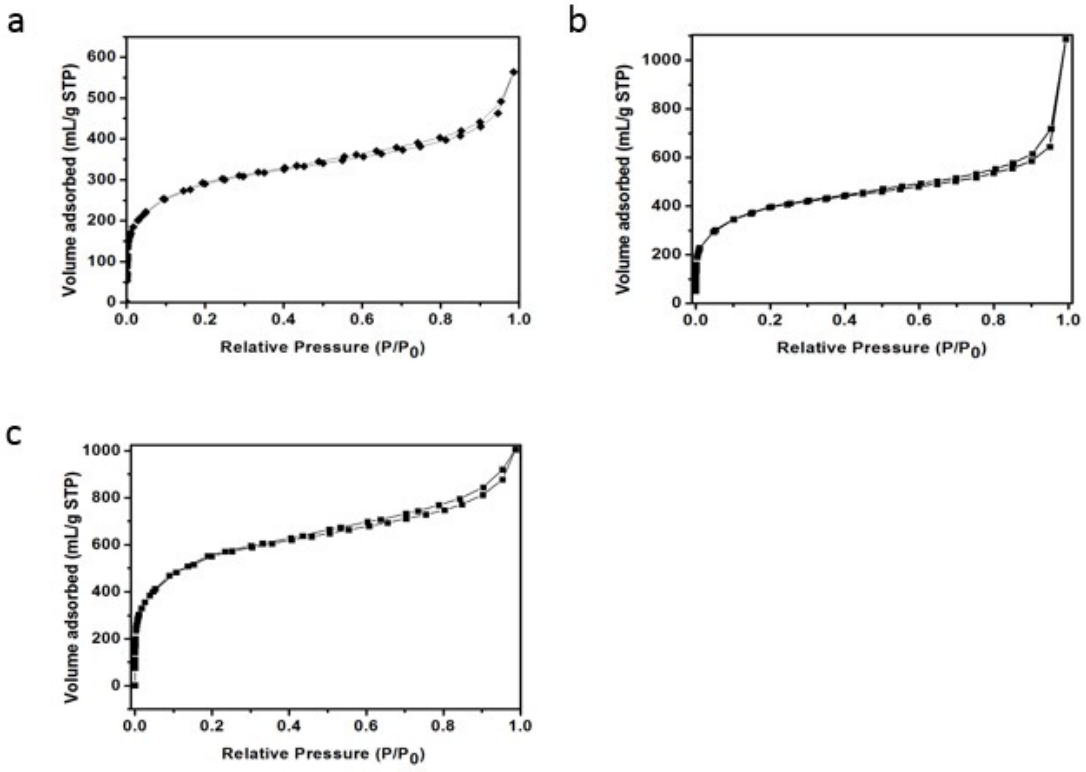

Figure S11. Nitrogen adsorption/desorption isotherms of Cr-MIL-101-NH_2, BET surface area of 1039 m^2 g^{-1} (a), 1452 m^2 g^{-1} (b), and 1989 m^2 g^{-1} (c).

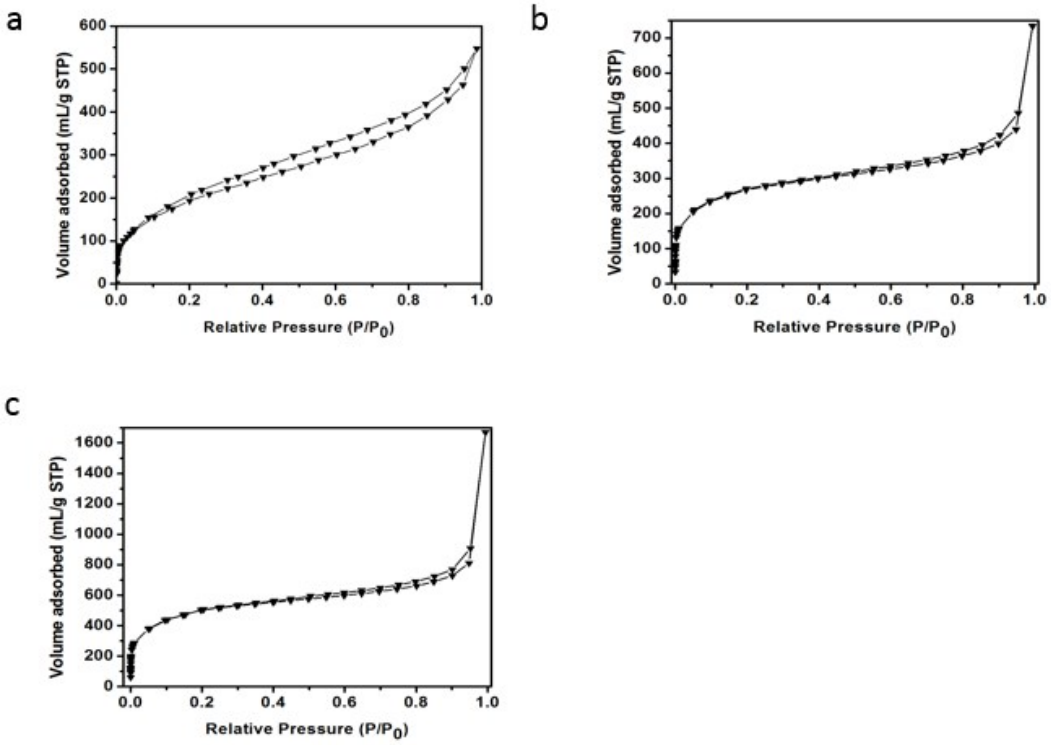

Figure S12. Nitrogen adsorption/desorption isotherms of Cr-MIL-101-NH-RNH_2, BET surface area of Cr-MIL-101-NH-RNH_2-1, 717 m^2 g^{-1} (a), Cr-MIL-101-NH-RNH_2-2 751 m^2 g^{-1} (b), and Cr-MIL-101-NH-RNH_2-3 1175 m^2 g^{-1} (c).

TGA

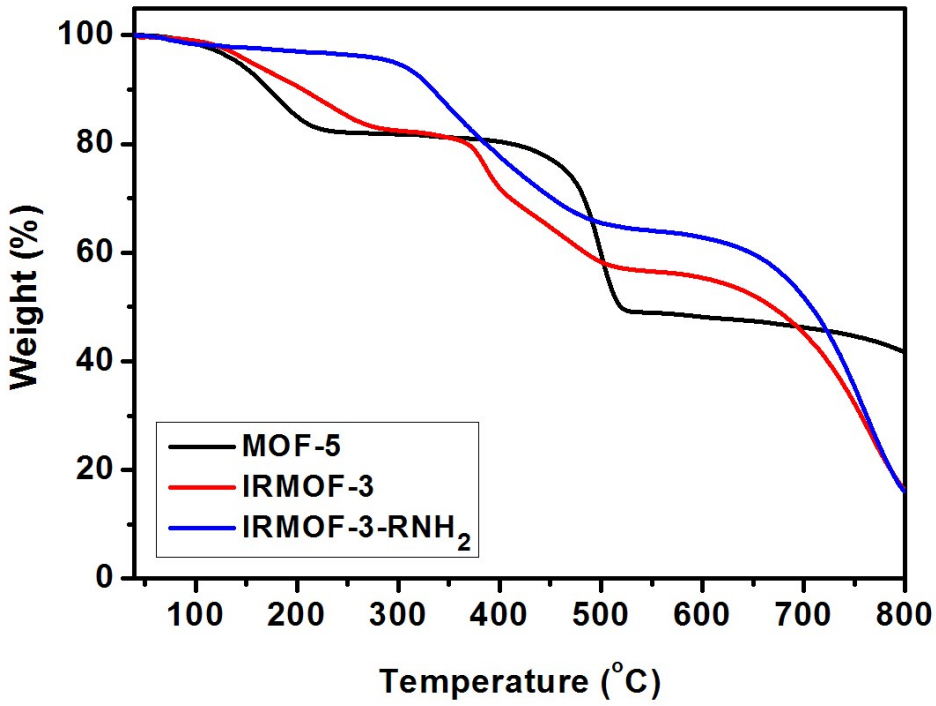

Figure S13. TGA of MOF5, IRMOF-3 and IRMOF-3-RNH_2

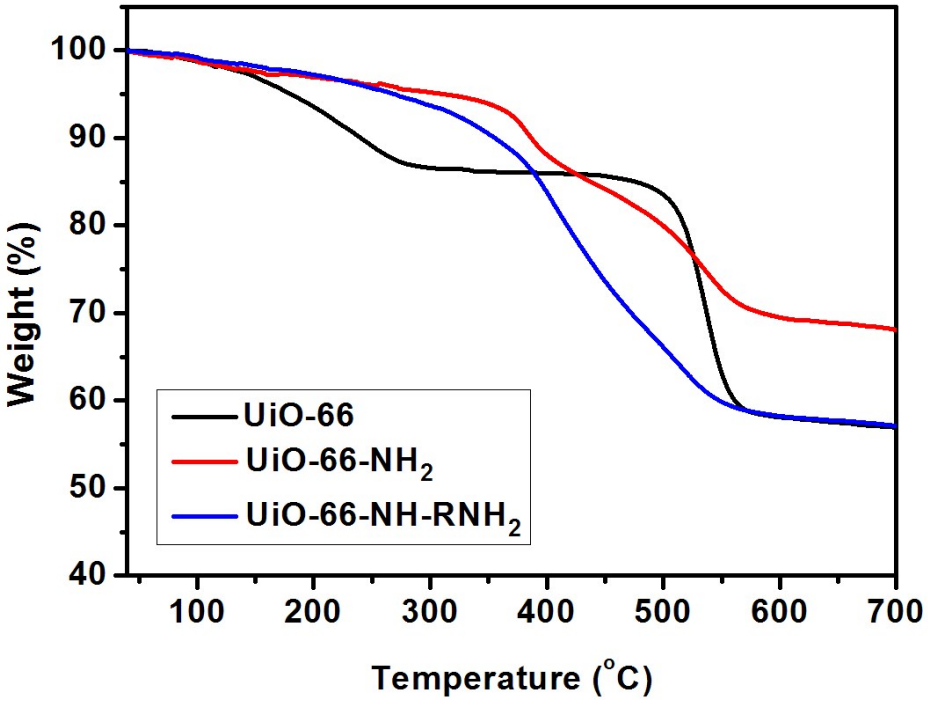

Figure S14. TGA of UiO-66, UiO-66-NH_2 and UiO-66-NH-RNH_2

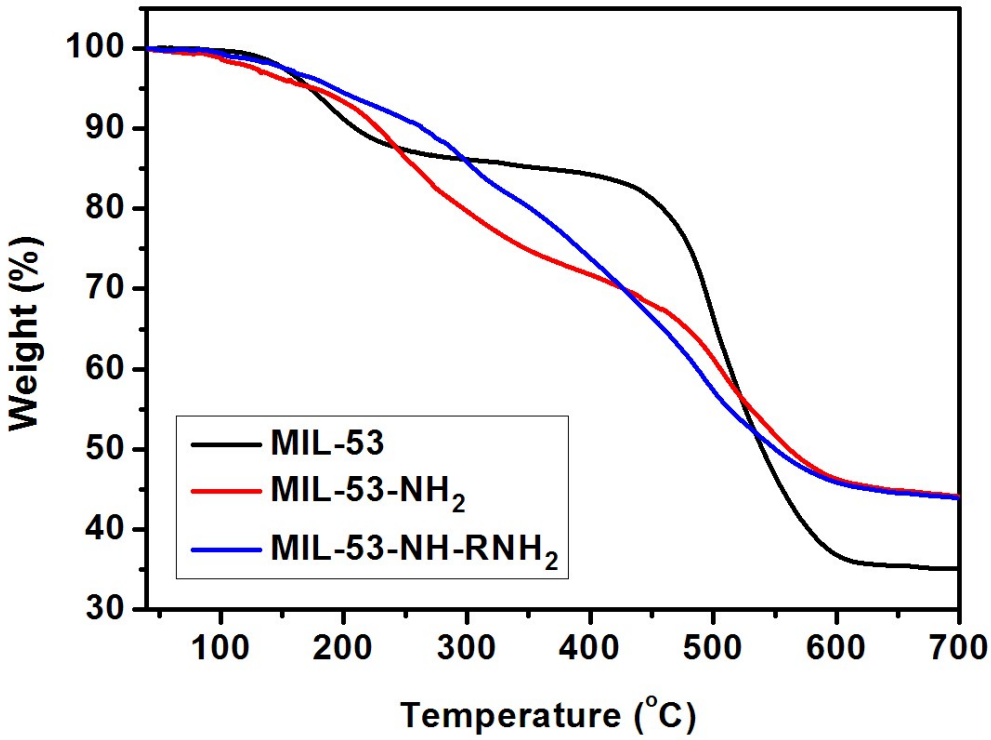

Figure S15. Al-53, Al-MIL-53-NH_2 and Al-MIL-53-NH-RNH_2

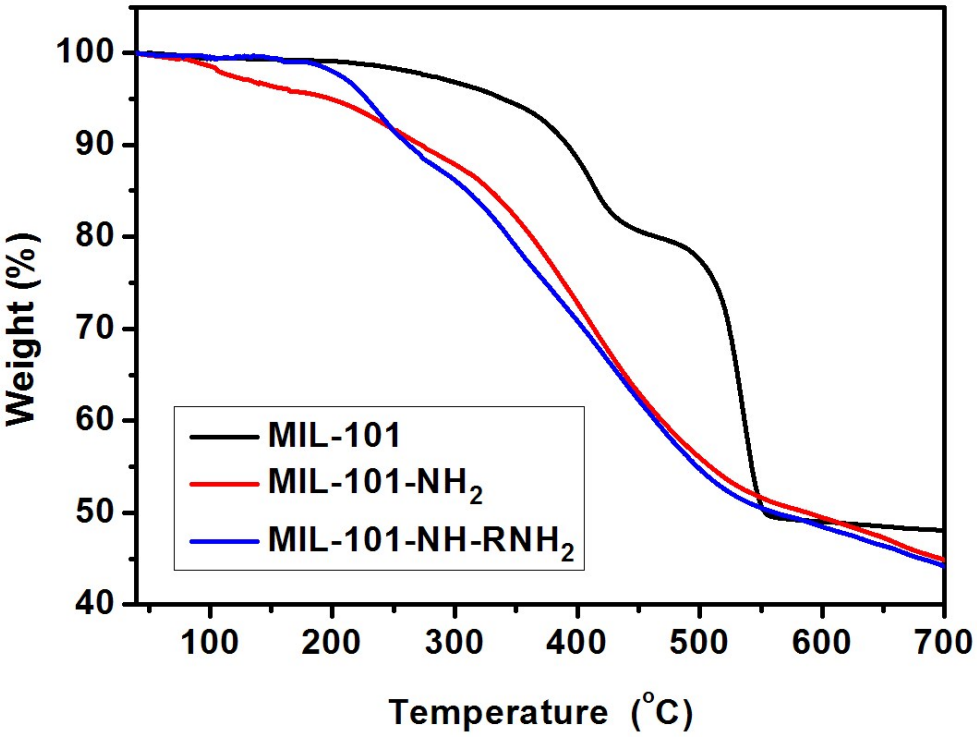

Figure S16. Cr-MIL-101, Cr-MIL-101-NH_2 and Cr-MIL-101-NH-RNH_2

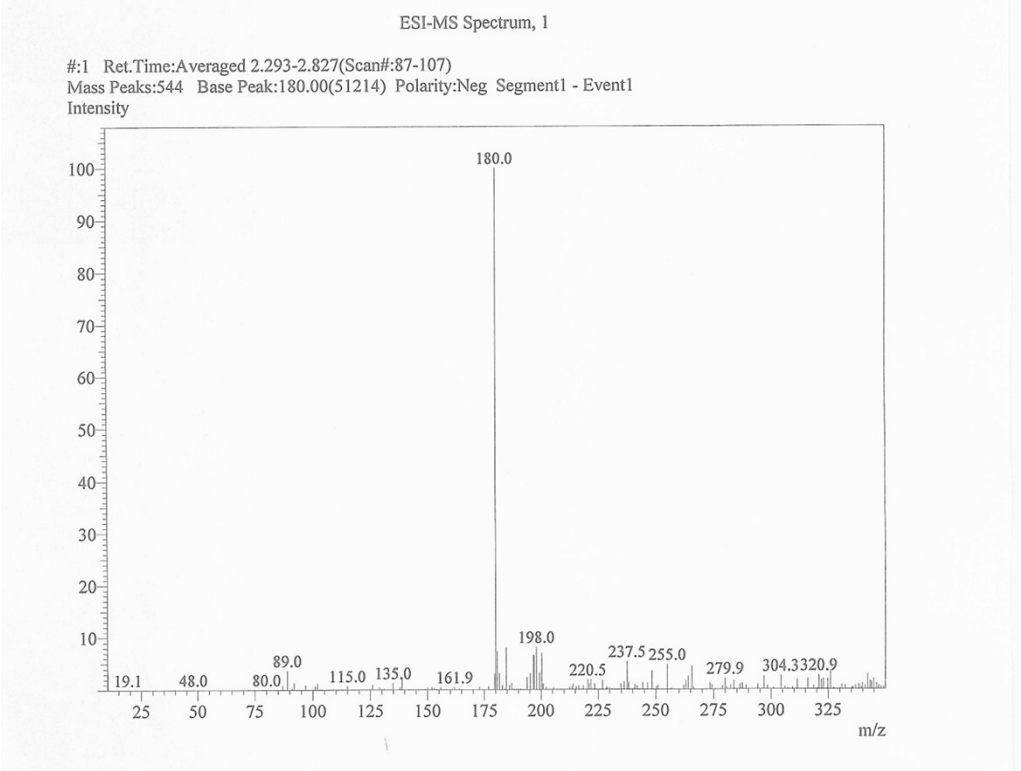

Figure S17. ESI-MS (negative mode) of IRMOF-3-RNH_2

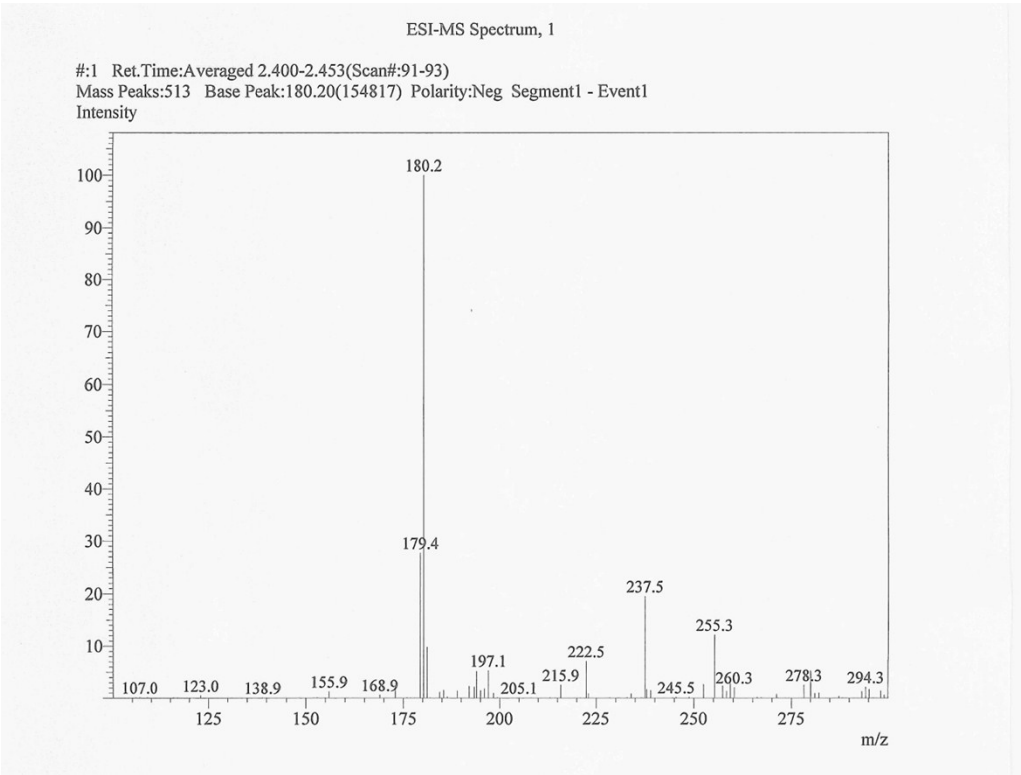

Figure S18. ESI-MS (negative mode) of UiO-66-NH-RNH_2

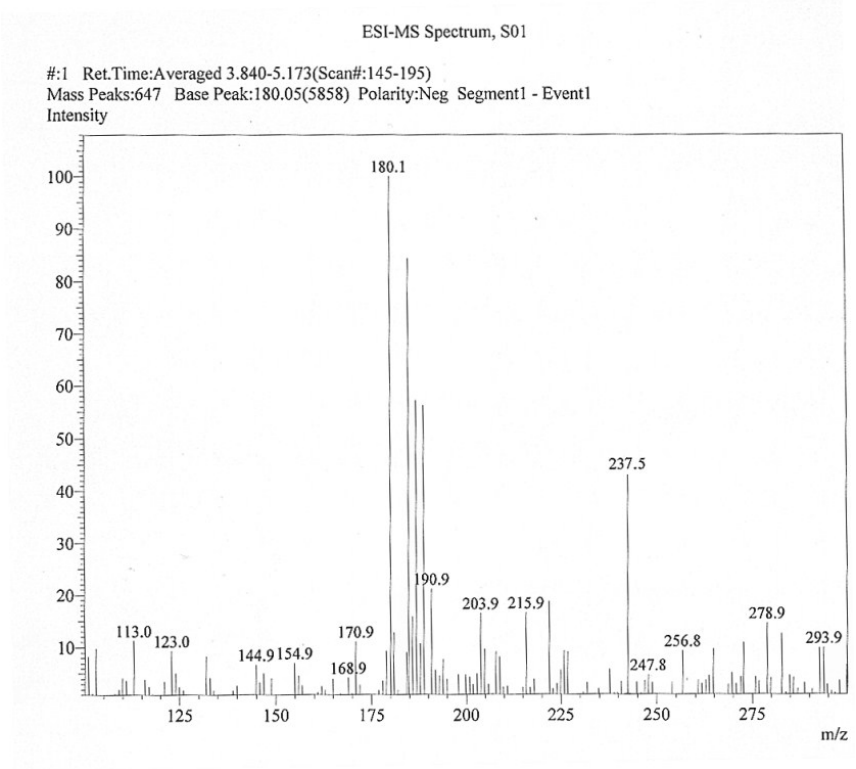

Figure S19. ESI-MS (negative mode) of Al-MIL-53-NH-RNH$_2$

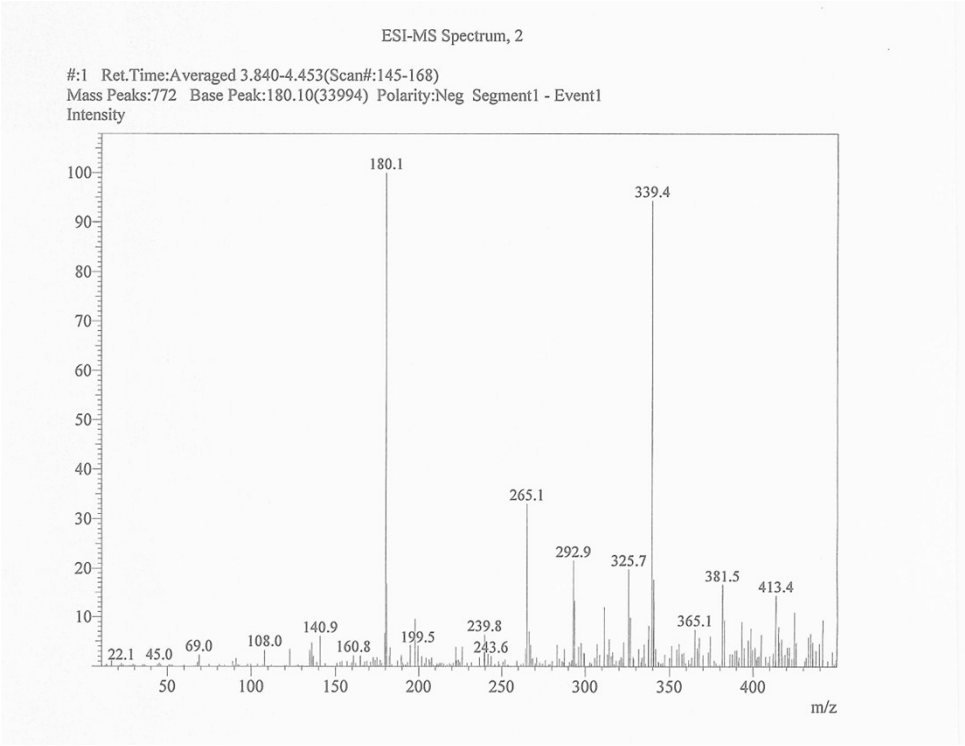

Figure S20. ESI-MS (negative mode) of Cr-MIL-101-NH-RNH$_2$

Catalytic material recycling characterizations

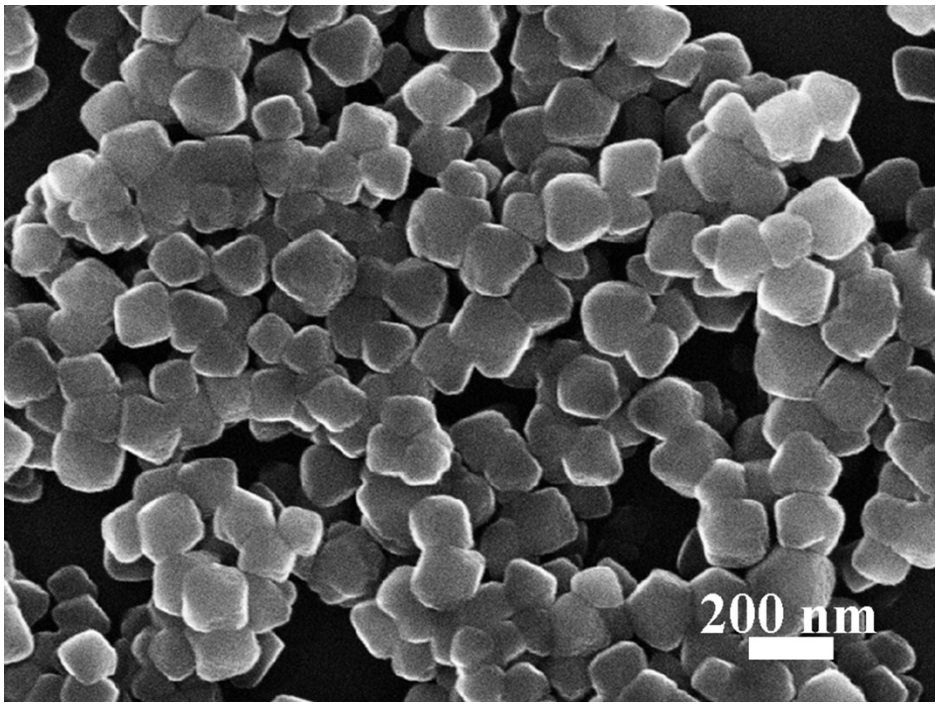

Figure 21. SEM images of recycled UiO-66-NH-RNH_2

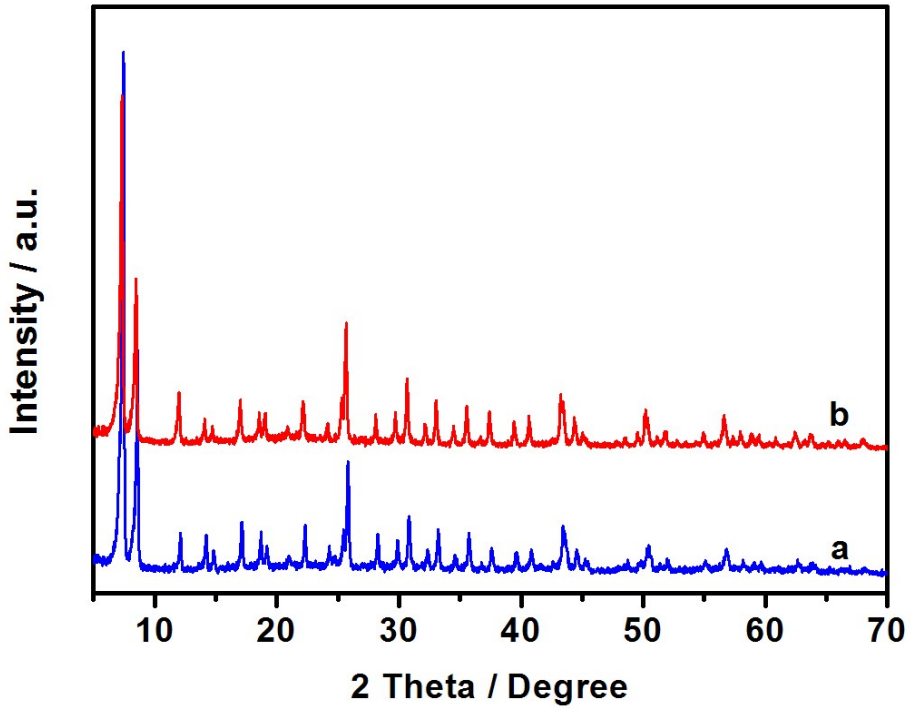

Figure 22. The XRD patterns of (a) fresh UiO-66-NH-RNH_2, (b) recycled UiO-66-NH-RNH_2.

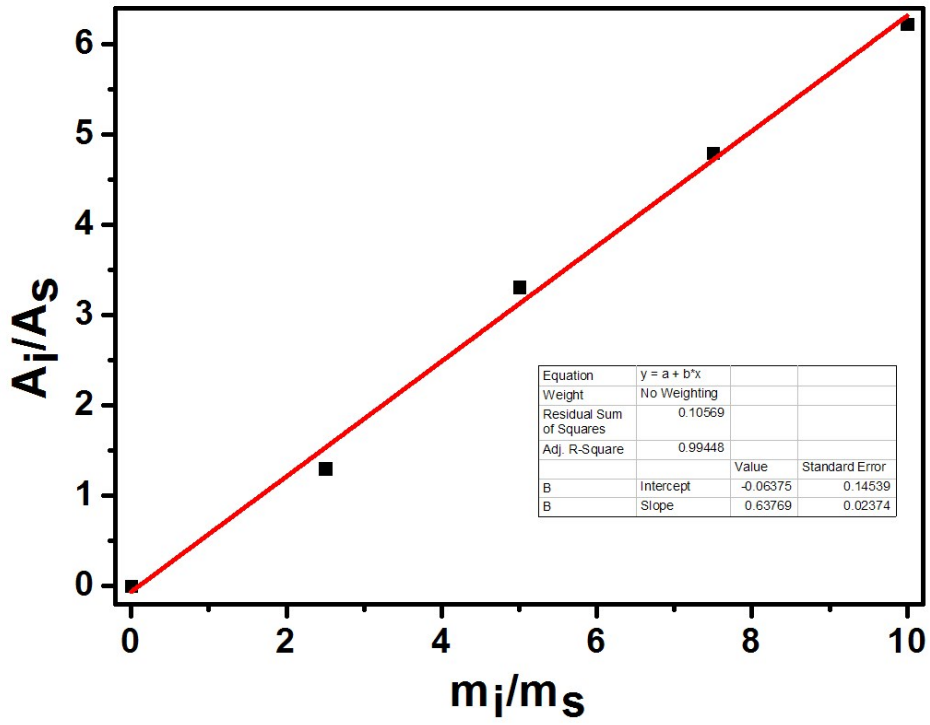

Figure 23. Benzaldehyde vs. *n*-dodecane internal standard for GC analysis

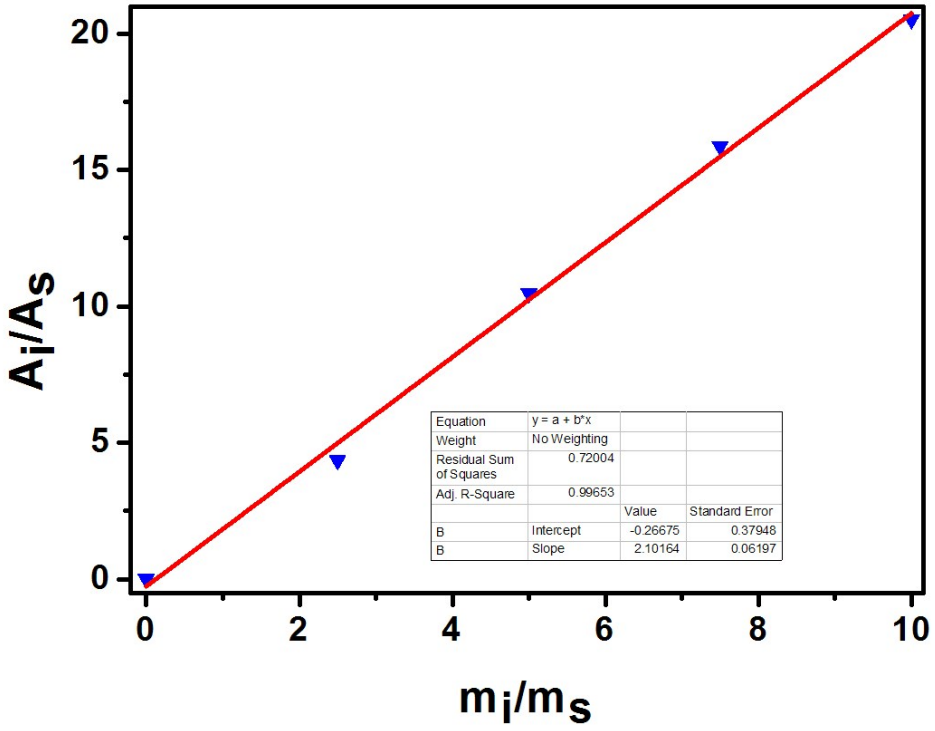

Figure 24. 2-benzylidenemalononitrile vs. *n*-dodecane internal standard for GC analysis

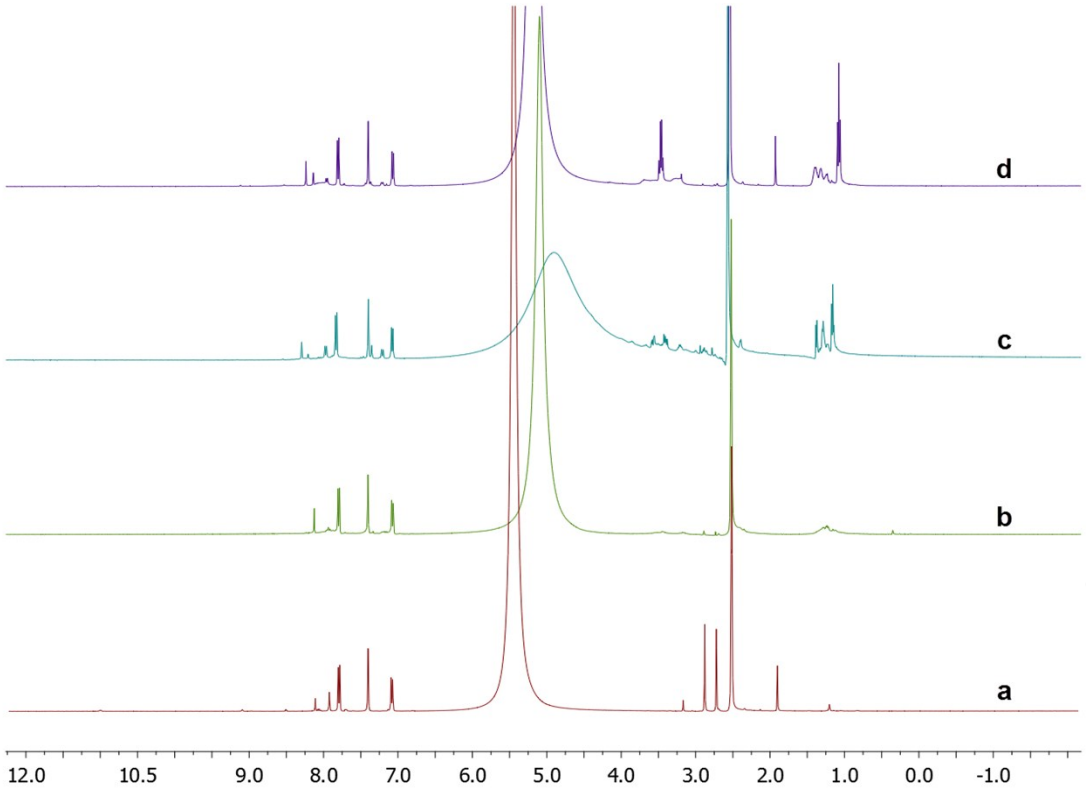

Figure S25. Full 1H NMR of MOFs, a) digested UiO-66, b) digested IRMOF-3-RNH_2, c) digested UiO-66-NH-RNH_2, d) digested Al-MIL-53-NH-RNH_2.

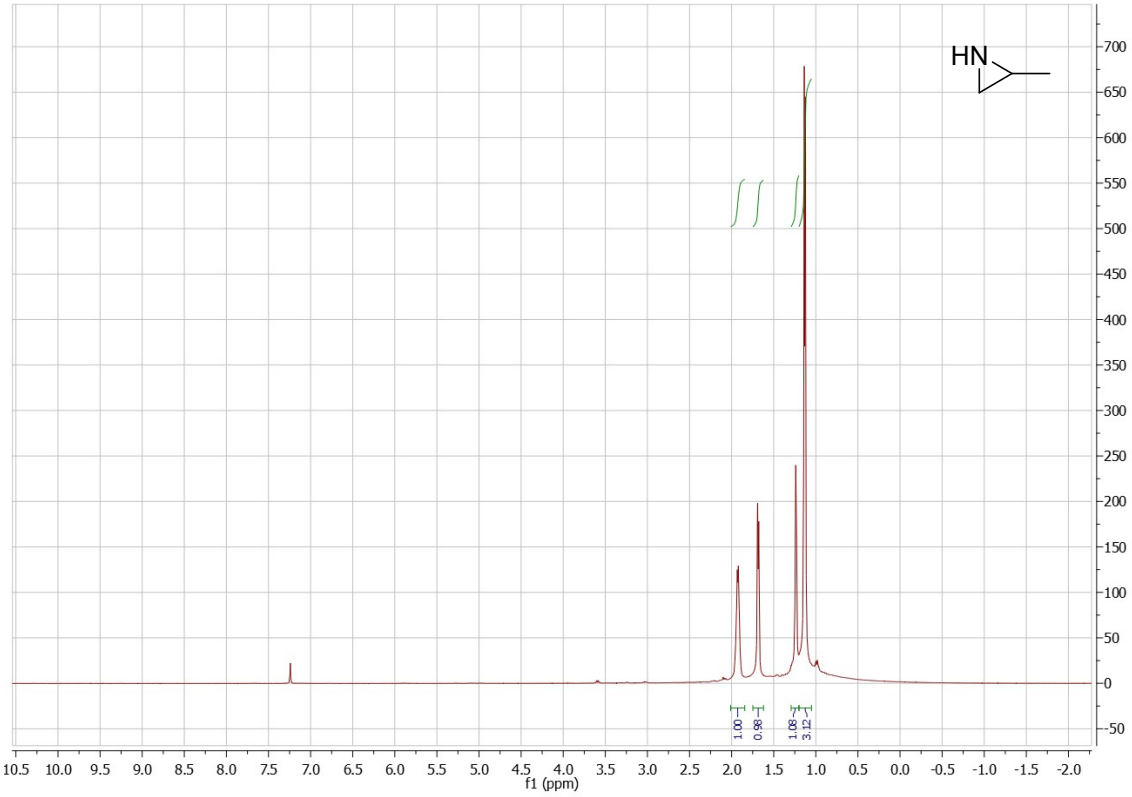

Figure S26. ^{1}H NMR of 2-methylaziridine

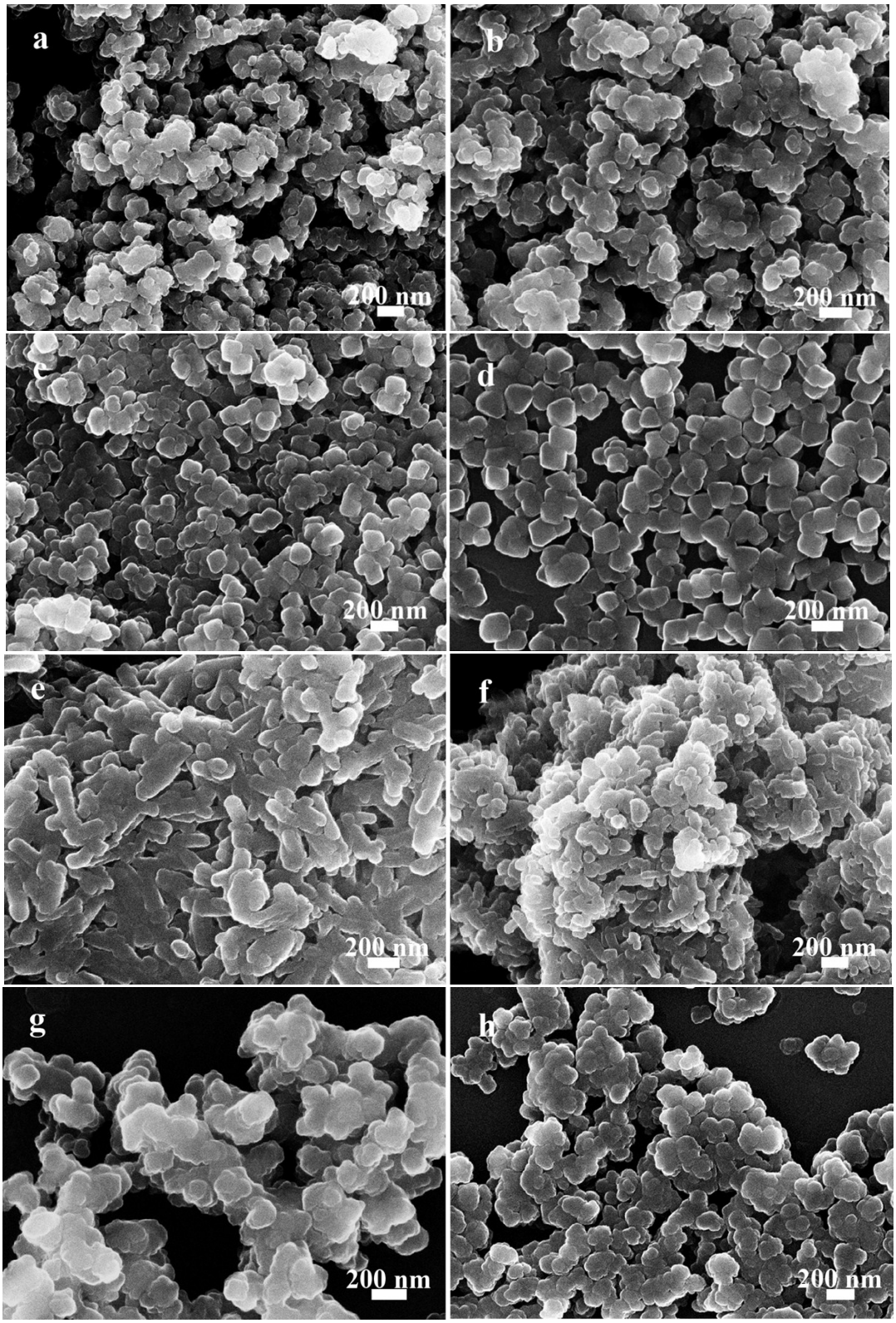

Fig. S27 SEM images of amino-tagged and basic modified MOF catalysts. (a) IRMOF-3, (b) IRMOF-3-RNH_2, (c) UiO-66-NH_2, (d) UiO-66-NH-RNH_2, (e) Al-MIL-53-NH_2, (f) Al-MIL-53-NH-RNH_2, (g) Cr-MIL-101-NH_2, (h) Cr-MIL-101-NH-RNH_2.

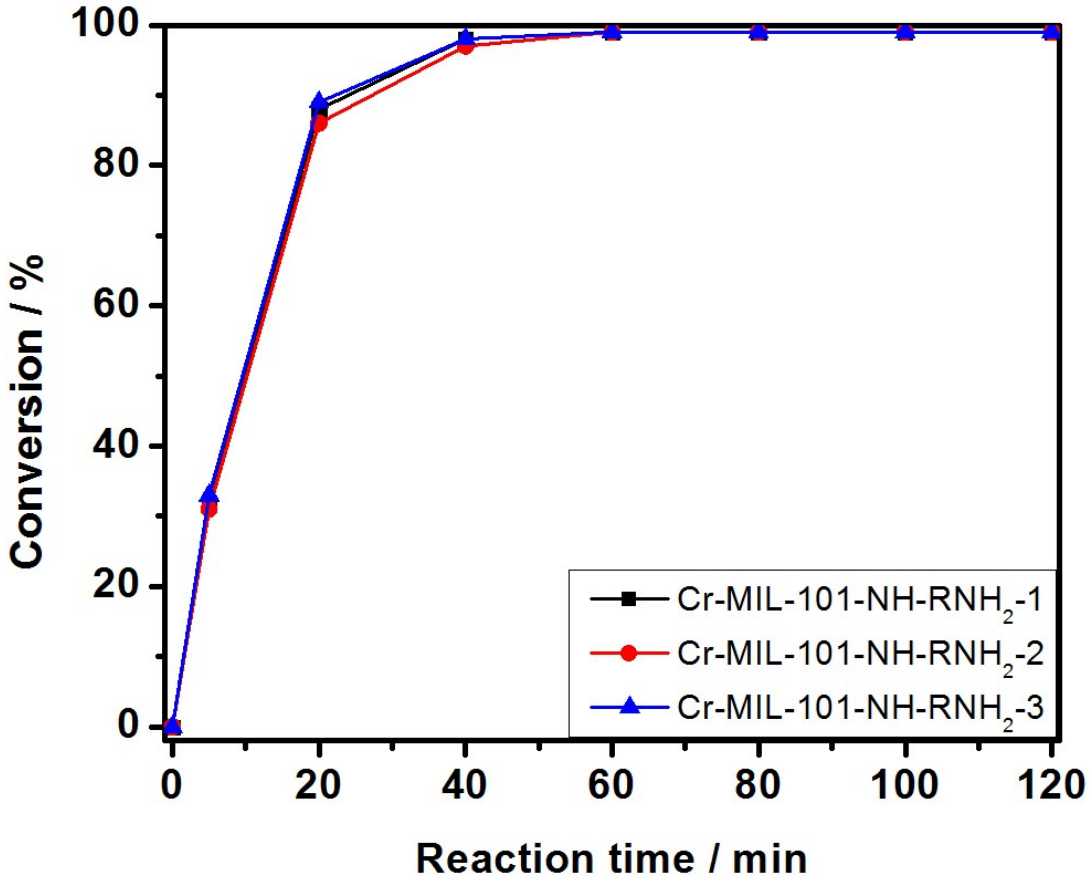

Fig. S28 Conversion vs. time employing Cr-MIL-101-NH-RNH_2 MOF catalyst.

Table S1. A comparison of catalytic activity of different catalysts in Knoevenagel condensation.

Entry	Catalyst	Mol%	Time	Solvent	Temp (ºC)	Yield	TON	TOF (h^{-1})	Ref.
1	PS-MCM-41	1	3 h	-	110	70%	70	23	1
2	MCM zeolite	17	3 h	Toluene	80	85%	5.0	1.7	2
3	SBA-15 zeolite	17	3 h	Toluene	80	88%	5.2	1.7	2
4	Nitrided ITQ-2	17	3 h	Toluene	80	95%	5.6	1.9	2
5	MgO	17	25 h	Toluene	80	45%	2.6	0.1	2
6	mesoporous $Ce_xZr_{1-x}O_2$	10	50 min	Ethanol	80	82%	8.2	9.9	3
7	ZIF-8	5	3 h	Toluene	r.t.	99%	20	6.7	4
8	ZIF-9	5	4 h	Toluene	r.t.	96%	19	4.8	5
9	TMU-5	2	30 min	H_2O	r.t.	100%	50	100	6
10	$[Gd_2(tnbd)_3\cdot(DMF)_4]\cdot 4DMF\cdot 3H_2O$	10	20 min	Benzene	r.t.	96%	9.6	48	7
11	$Pd(cpna)_2\cdot 2DMF\cdot 6H_2O$	3	24 h	CH_3CN	r.t.	100%	33.3	1.4	8
12	DETA-MIL-101	Not indicated	0.5-2 h	Toluene	r.t.	18-98%	-	9-108	9
13	UiO-66-NH-RNH_2	1	2 h	Toluene	r.t.	99%	99	50	**This work**
14	Cr-MIL-101-NH-RNH_2	1	20 min	Toluene	r.t.	88%	88	264	**This work**
15	Cr-MIL-101-NH-RNH_2	1	5 min	Toluene	r.t.	33%	33	396	**This work**

[a] The mole percentage of PS-MCM-41, MCM zeolite, SBA-15 zeolite, Nitrided ITQ-2, ZIF-8, ZIF-9, TMU-5, DETA-MIL-101 (entries 1-4, 7-9 and 12) was calculated based on the active nitrogen.

[b] The mole percentage of MgO, mesoporous $Ce_xZr_{1-x}O_2$, $[Gd_2(tnbd)_3\cdot(DMF)_4]\cdot 4DMF\cdot 3H_2O$, $Pd(cpna)_2\cdot 2DMF\cdot 6H_2O$ was calculated based on the metal content (entries 5-6, 10-11).

[c] The mole percentage of our catalyst (entries 13-15) was calculated based on the alkyl amino group, which indicates substrate per active center.

[1] A. Corma, S. Iborra, I. Rodriguez and F. Sanchez, *J. Catal.*, 2002, **211**, 208-215.
[2] H. K. Min, S. H. Cha and S. B. Hong, *Chem. Commun.*, 2013, **49**, 1115-1117.
[3] G. Postole, B. Chowdhury, B. Karmakar, K. Pinki, J. Banerji and A. Auroux, *J. Catal.*, **269**, 110-121.
[4] U. P. N. Tran, K. K. A. Le and N. T. S. Phan, *ACS Catal.*, 2011, **1**, 120-127.

[5] L. T. L. Nguyen, K. K. A. Le, H. X. Truong and N. T. S. Phan, *Catal. Sci. Tech.*, 2012, **2**, 521-528.
[6] M. Y. Masoomi, S. Beheshtia and A. Morsali, *J. Mater. Chem. A*, 2014, **2**, 16863-16866.
[7] R. K. Das, A. Aijaz, M. K. Sharma, P. Lama and P. K. Bharadwaj, *Chem. Eur. J.*, 2012, **18**, 6866-6872.
[8] X. M. Lin, T. T. Li, L. F. Chen, L. Zhang and C. Y. Su, *Dalton Trans.*, 2012, **41**, 10422-10429.
[9] S. Na Kim, S. T. Yang, J. Kim, J. E. Park and W. S. Ahn, *CrystEngComm*, 2012, **14**, 4142–4147.

Gas-chromatogram Mass-spectrum

Table 3, Entry 1,

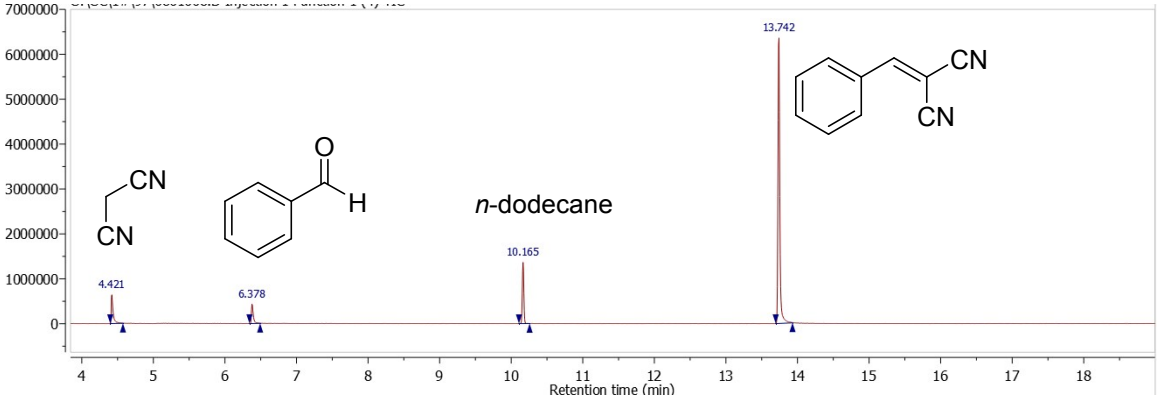

Catalyzed by UiO-66-NH-RNH$_2$

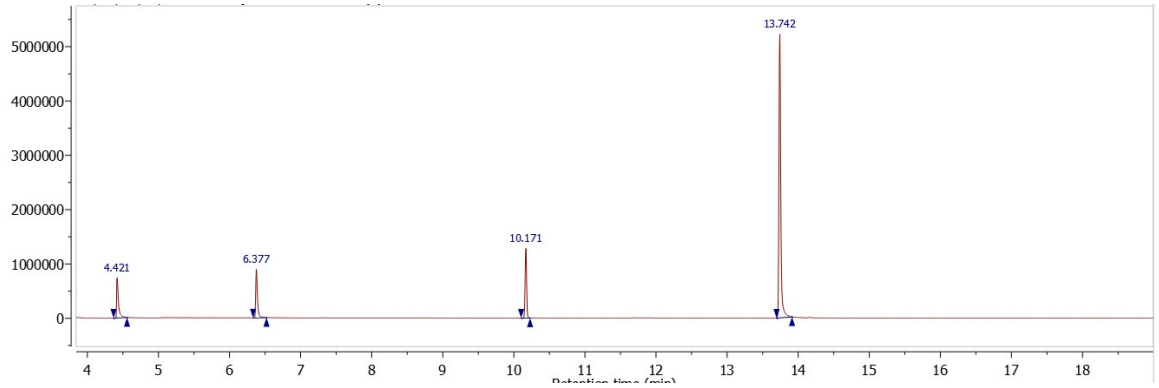

Catalyzed by Al-MIL-53-NH-RNH$_2$

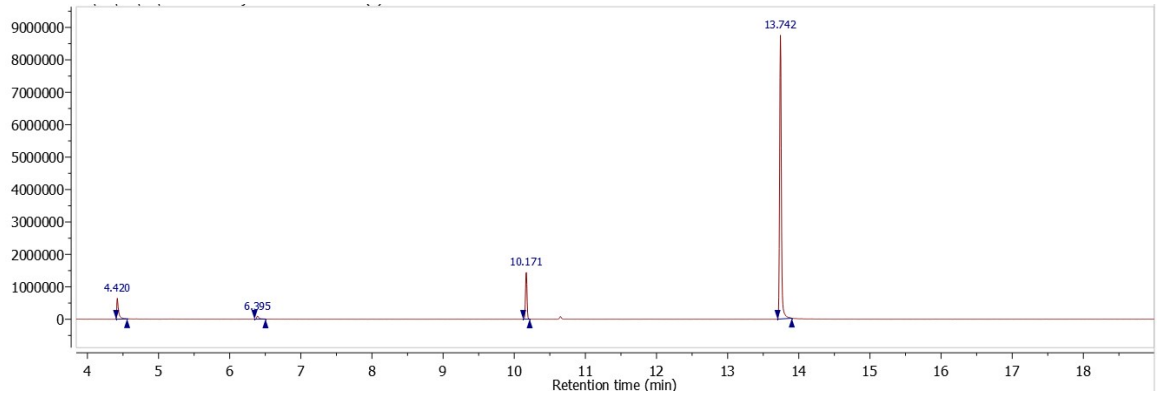

Catalyzed by Cr-MIL-101-NH-RNH$_2$

Table 3, Entry 2

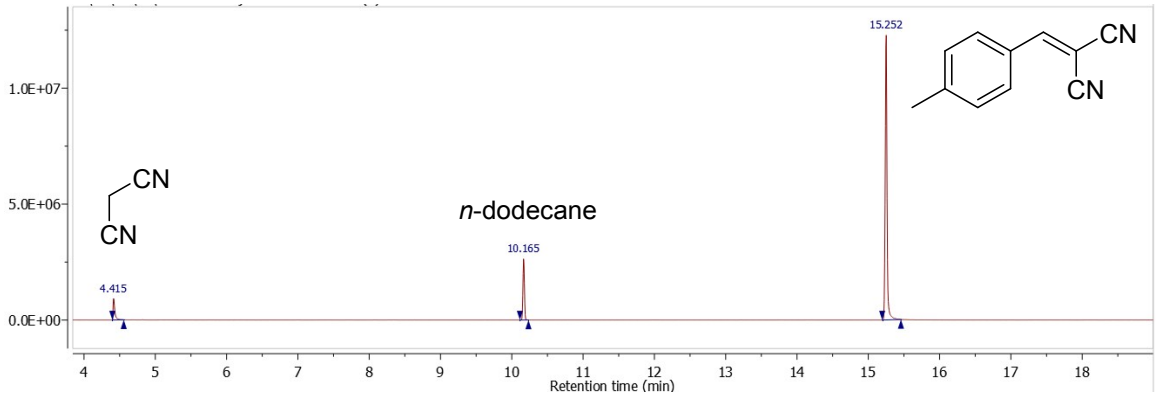

Catalyzed by UiO-66-NH-RNH_2

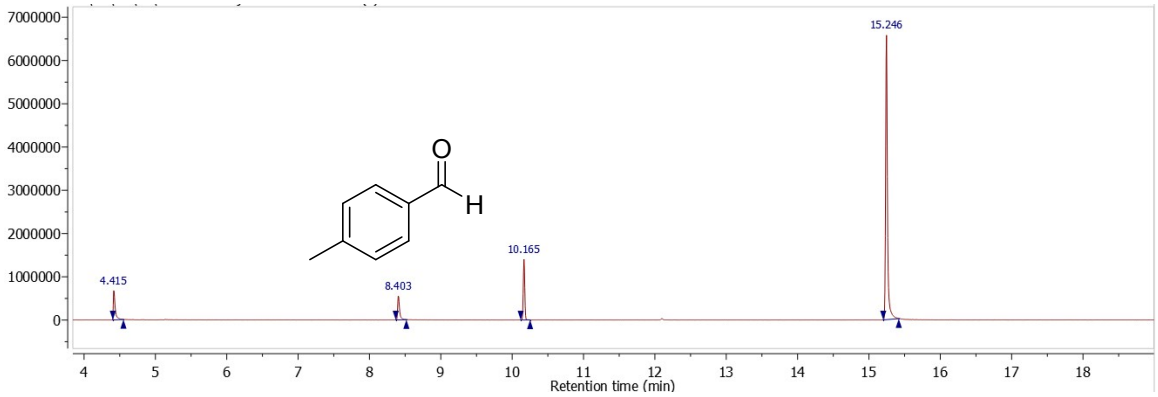

Catalyzed by Al-MIL-53-NH-RNH_2

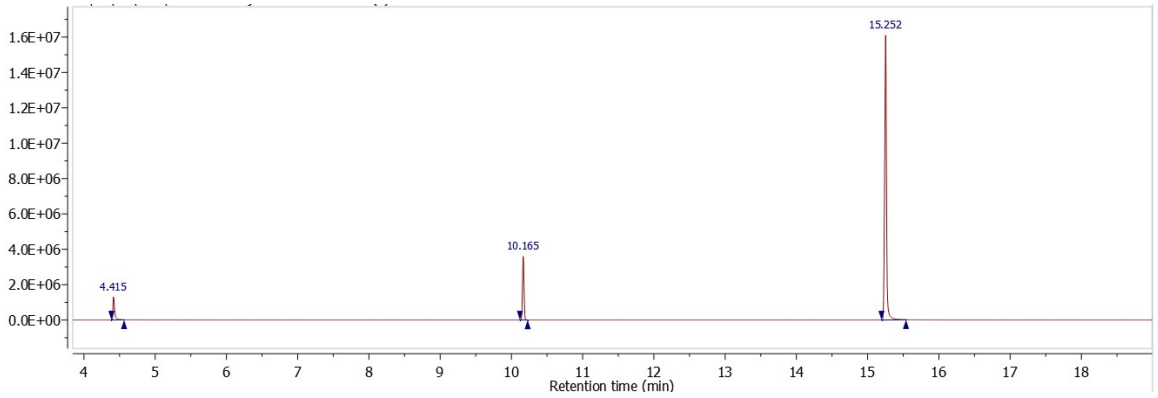

Catalyzed by Cr-MIL-101-NH-RNH_2

Table 3, Entry 3

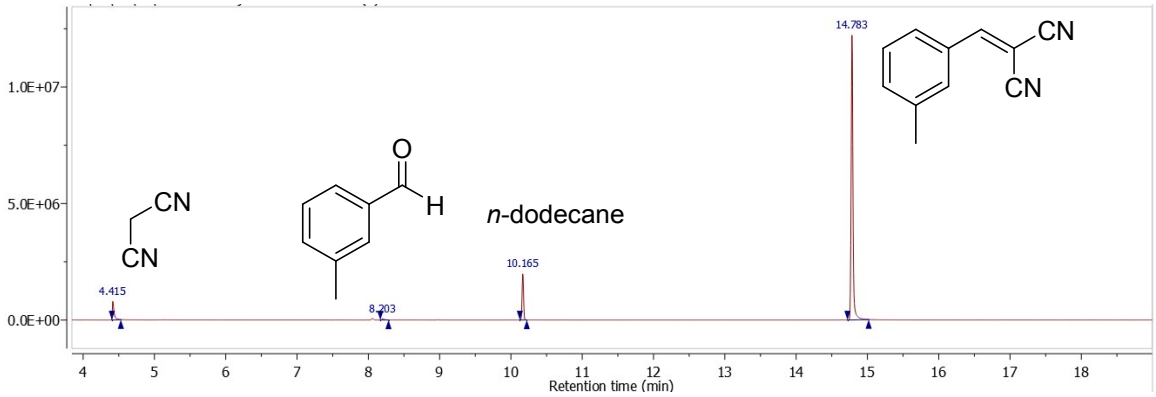

Catalyzed by UiO-66-NH-RNH_2

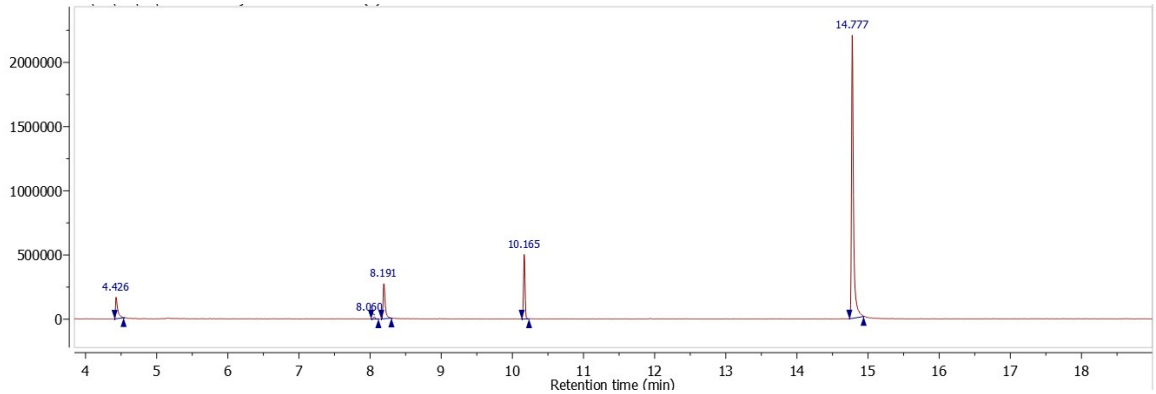

Catalyzed by Al-MIL-53-NH-RNH_2

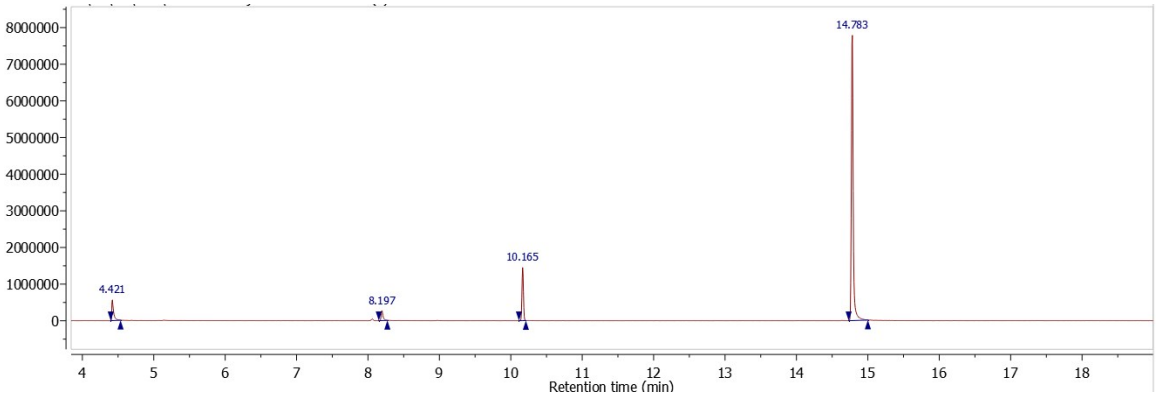

Catalyzed by Cr-MIL-101-NH-RNH_2

Table 3, Entry 4

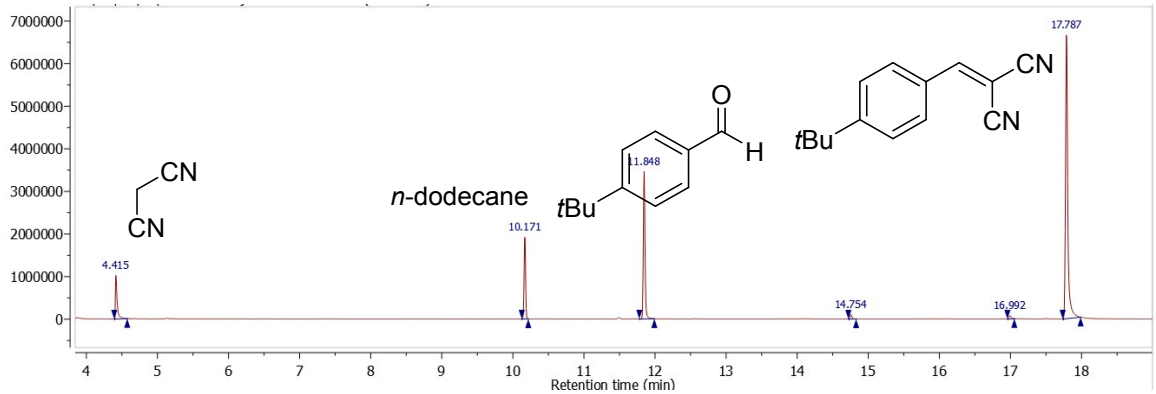

Catalyzed by UiO-66-NH-RNH_2

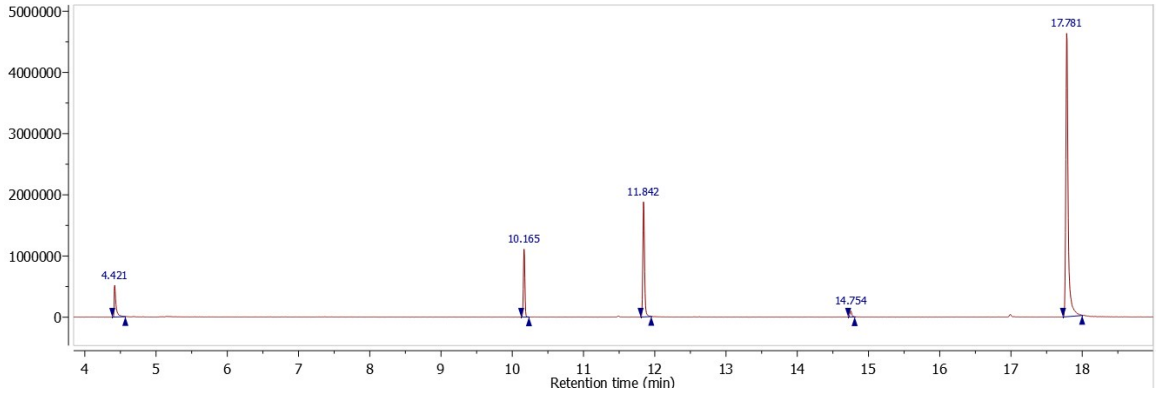

Catalyzed by Al-MIL-53-NH-RNH_2

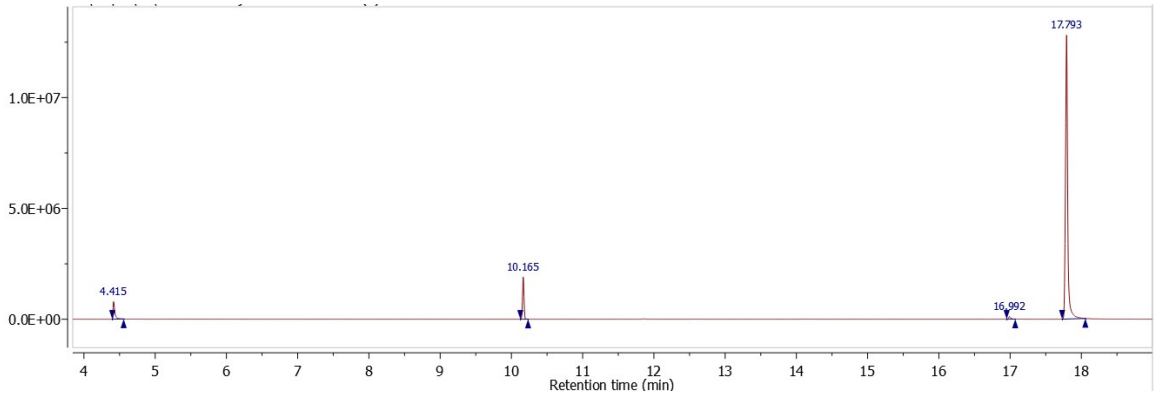

Catalyzed by Cr-MIL-101-NH-RNH_2

Table 3, Entry 5

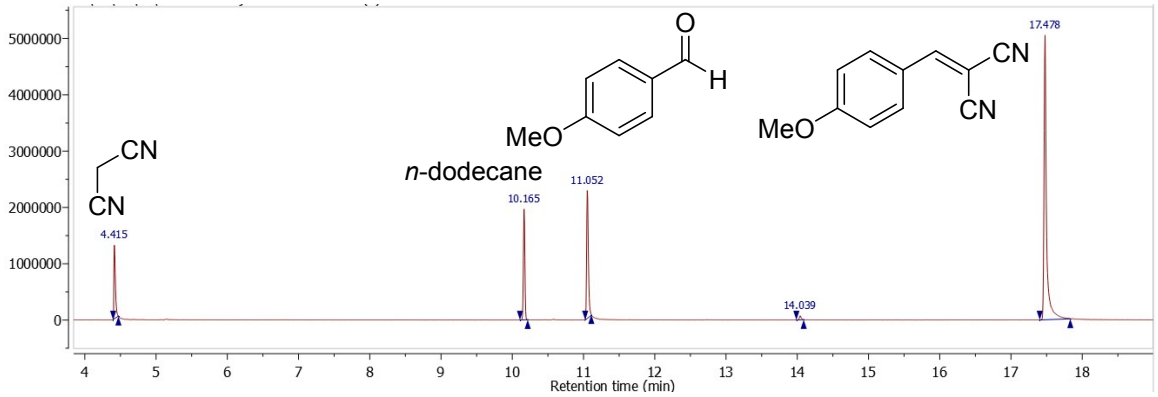

Catalyzed by UiO-66-NH-RNH_2

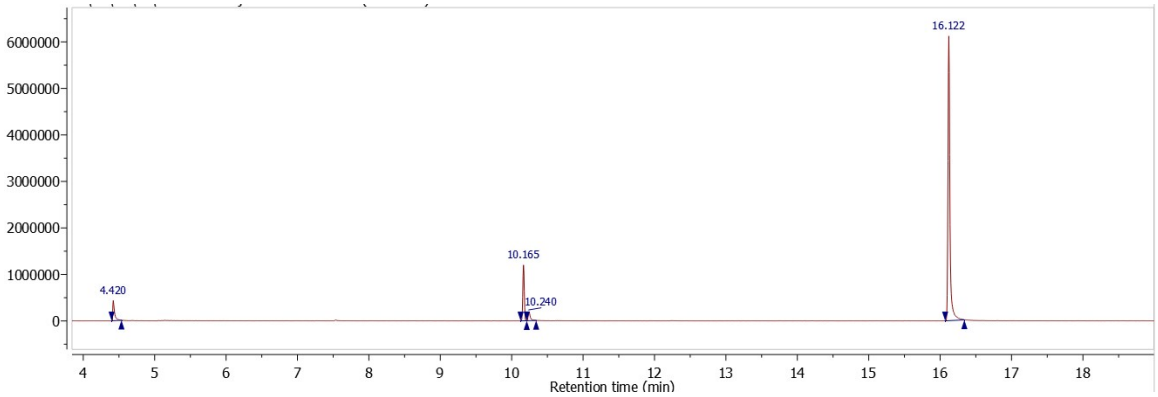

Catalyzed by Al-MIL-53-NH-RNH_2

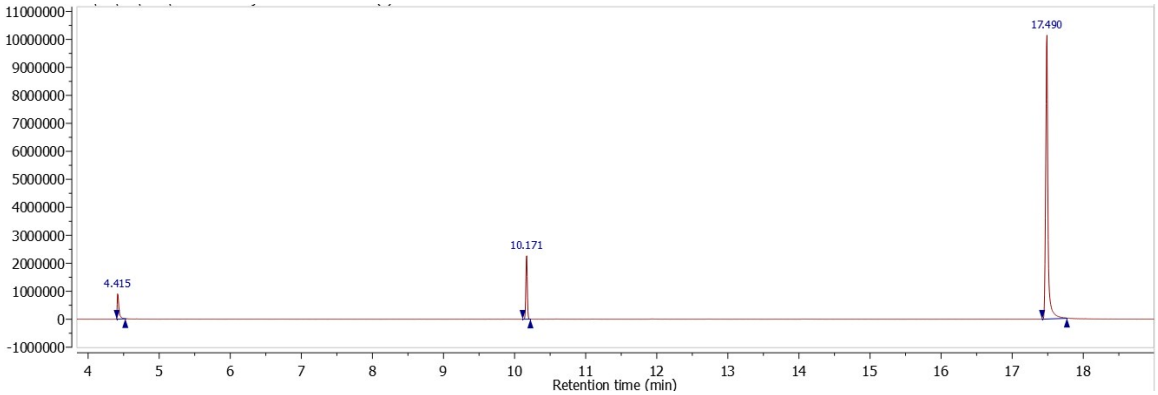

Catalyzed by Cr-MIL-101-NH-RNH_2

Table 3, Entry 6

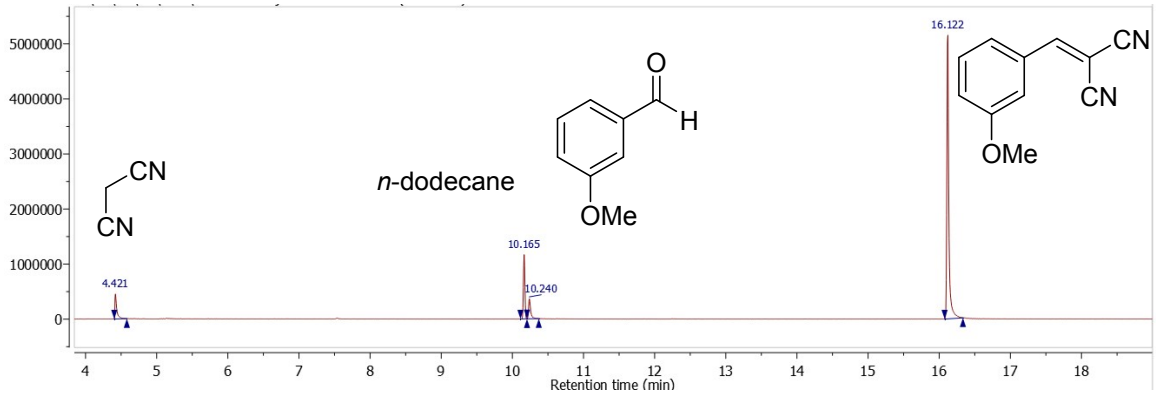

Catalyzed by UiO-66-NH-RNH_2

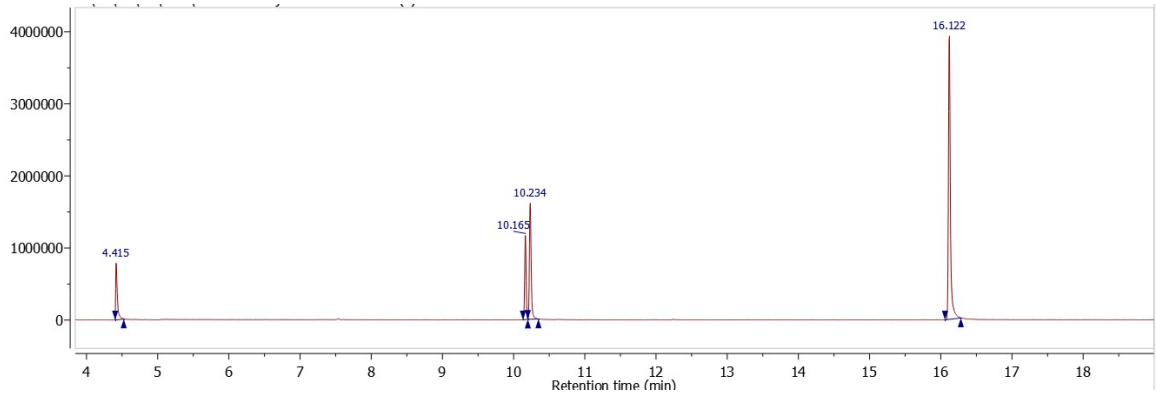

Catalyzed by Al-MIL-53-NH-RNH_2

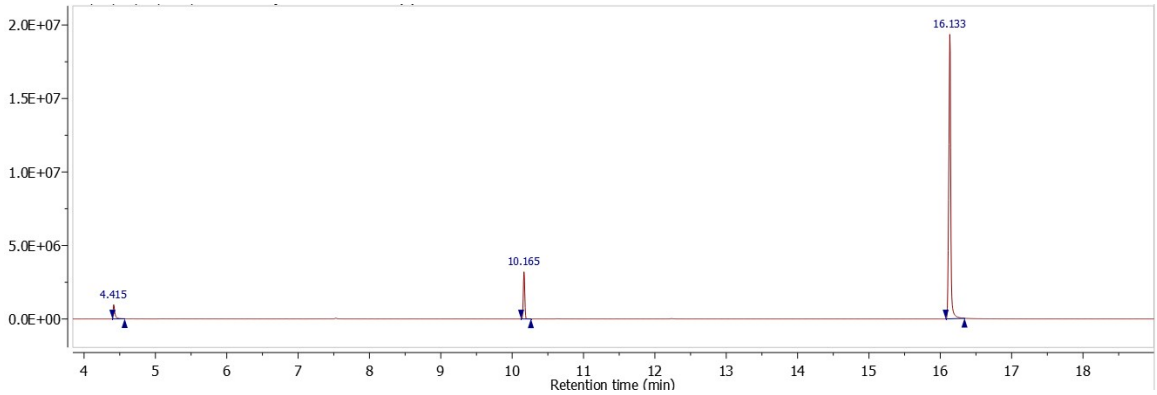

Catalyzed by Cr-MIL-101-NH-RNH_2

Table 3, Entry 7

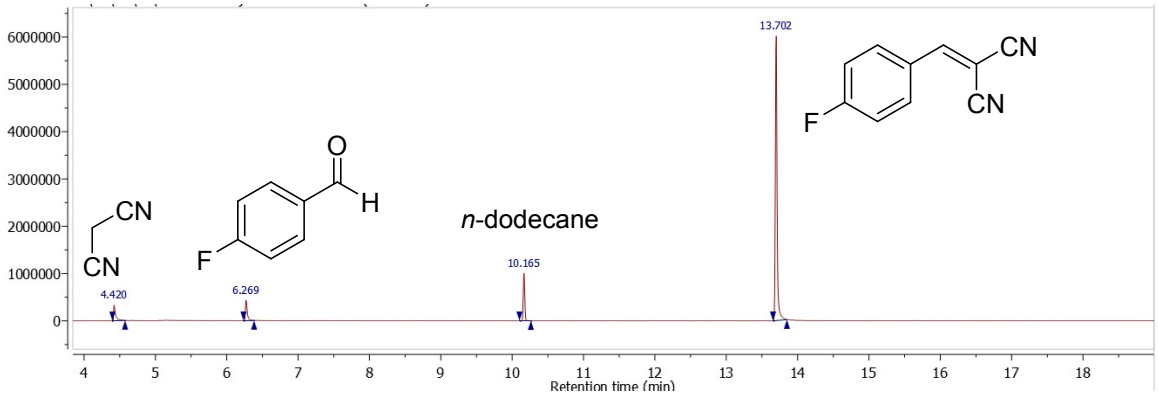

Catalyzed by UiO-66-NH-RNH_2

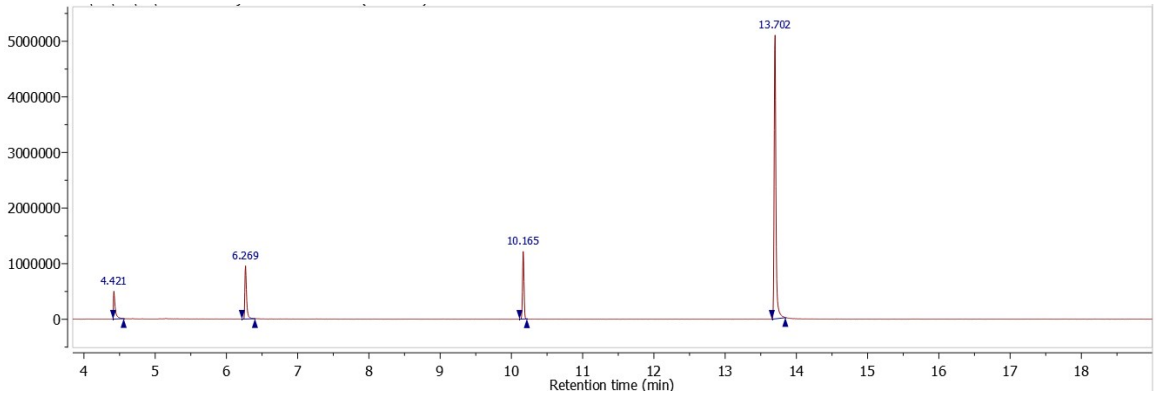

Catalyzed by Al-MIL-53-NH-RNH_2

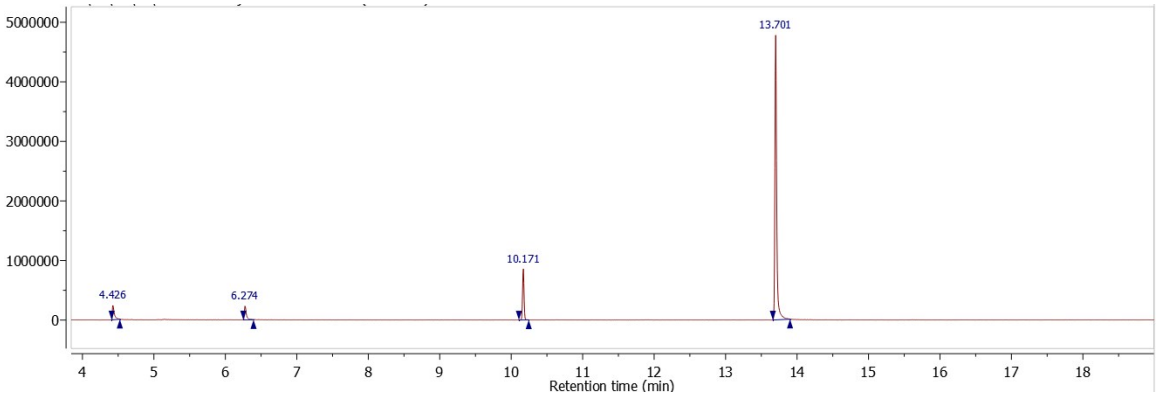

Catalyzed by Cr-MIL-101-NH-RNH_2

Table 3, Entry 8,

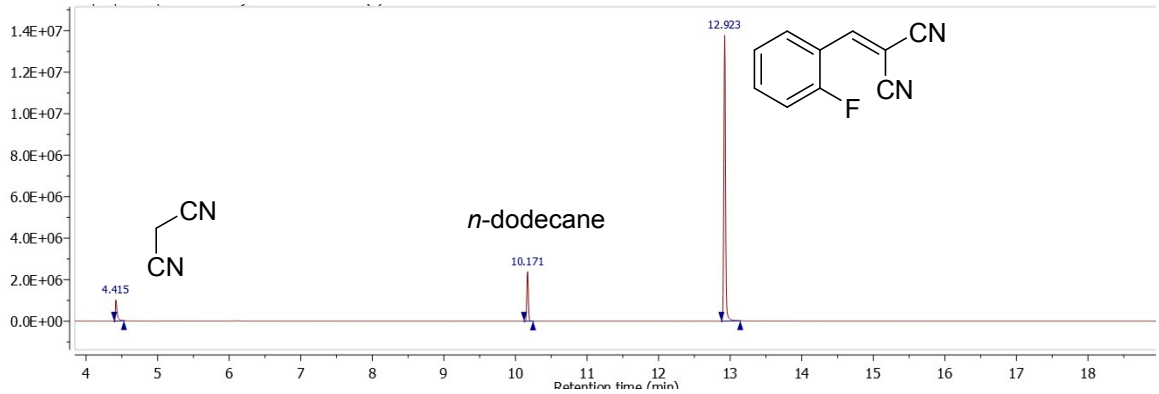

Catalyzed by UiO-66-NH-RNH_2

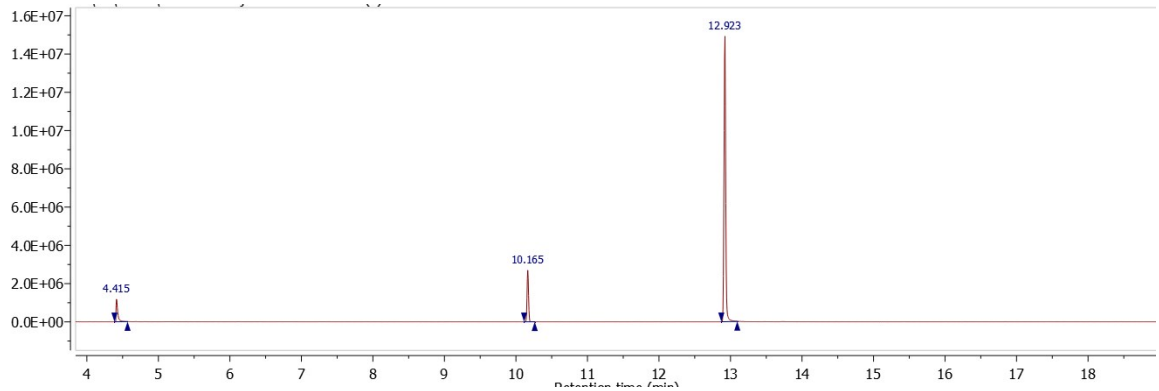

Catalyzed by Al-MIL-53-NH-RNH_2

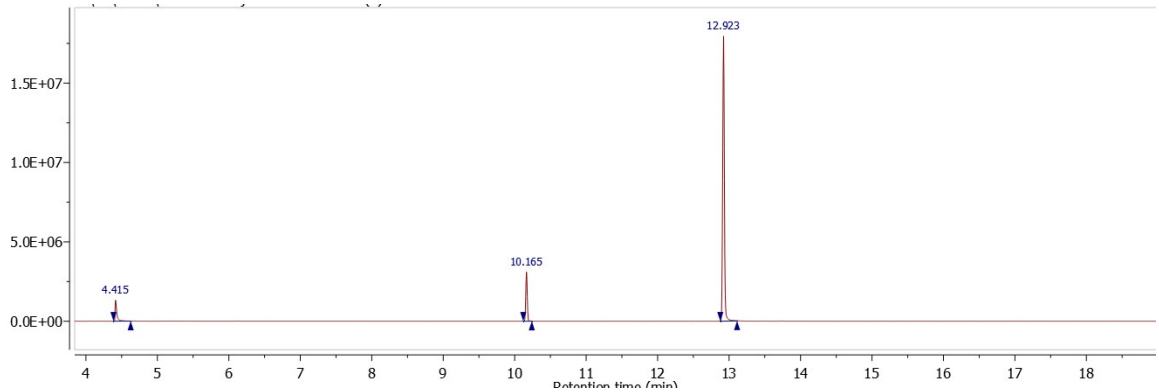

Catalyzed by Cr-MIL-101-NH-RNH_2

Table 3, Entry 9

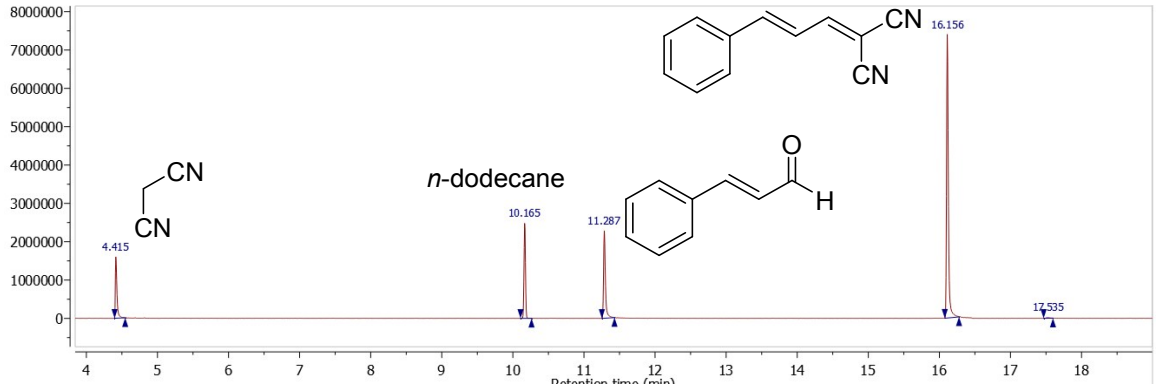

Catalyzed by UiO-66-NH-RNH_2

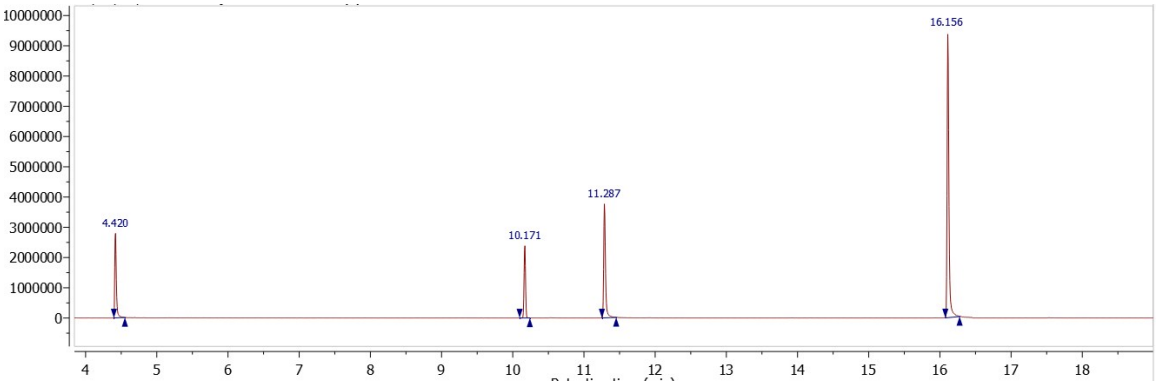

Catalyzed by Al-MIL-53-NH-RNH_2

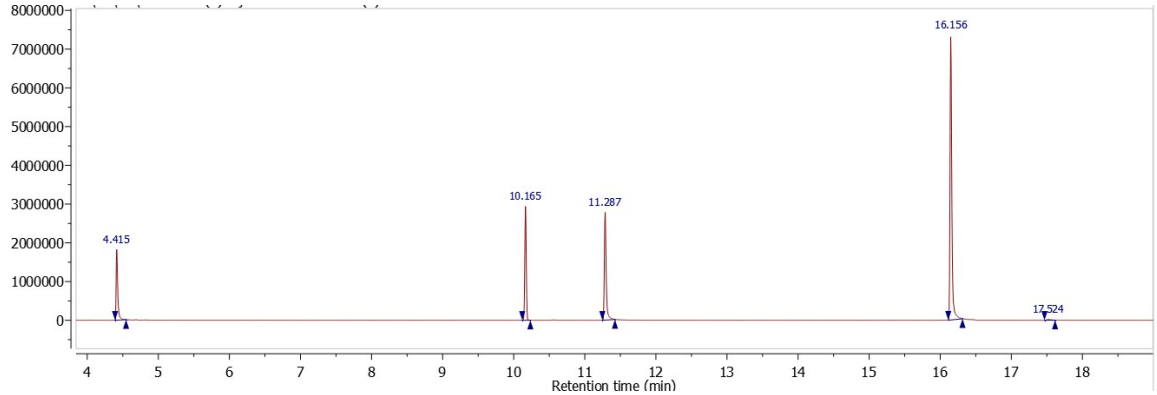

Catalyzed by Cr-MIL-101-NH-RNH_2

Table 3, Entry 10,

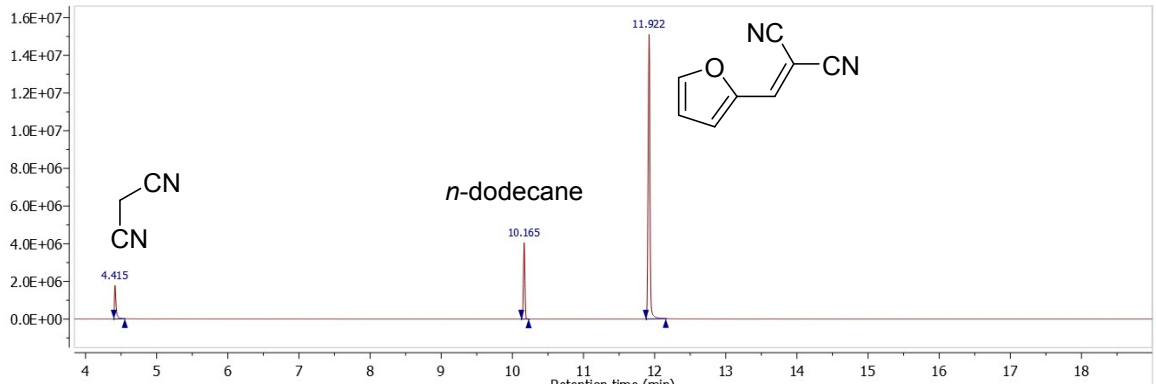

Catalyzed by UiO-66-NH-RNH_2

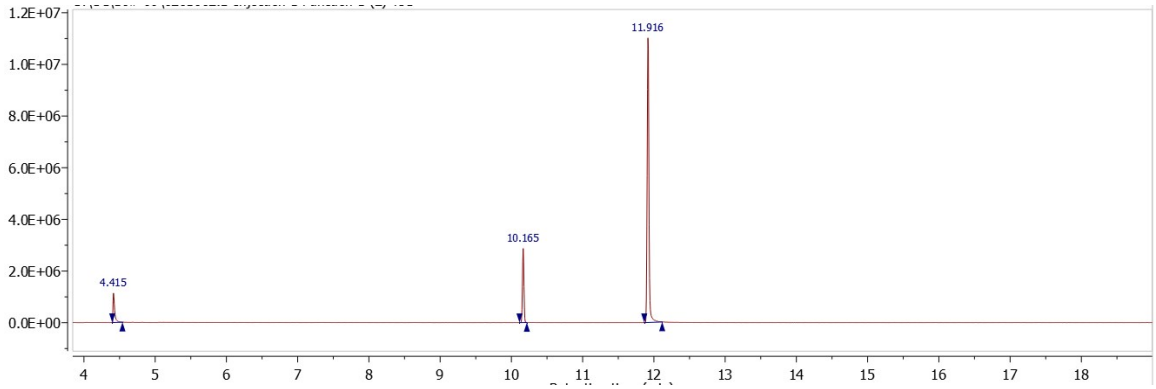

Catalyzed by Al-MIL-53-NH-RNH_2

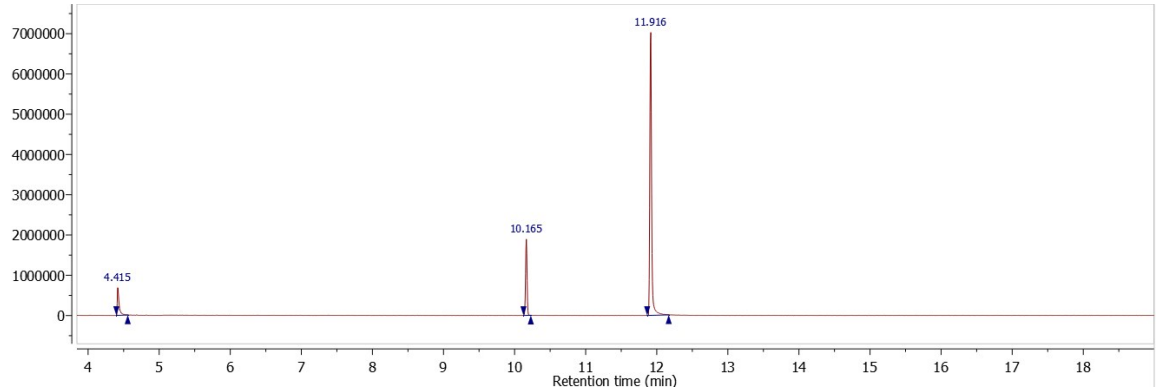

Catalyzed by Cr-MIL-101-NH-RNH_2

Table 3, Entry 11

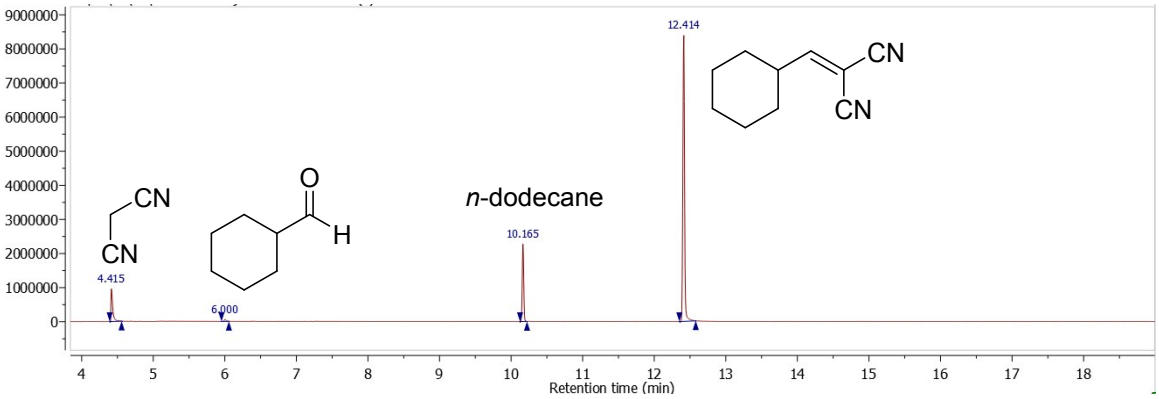

Catalyzed by UiO-66-NH-RNH_2

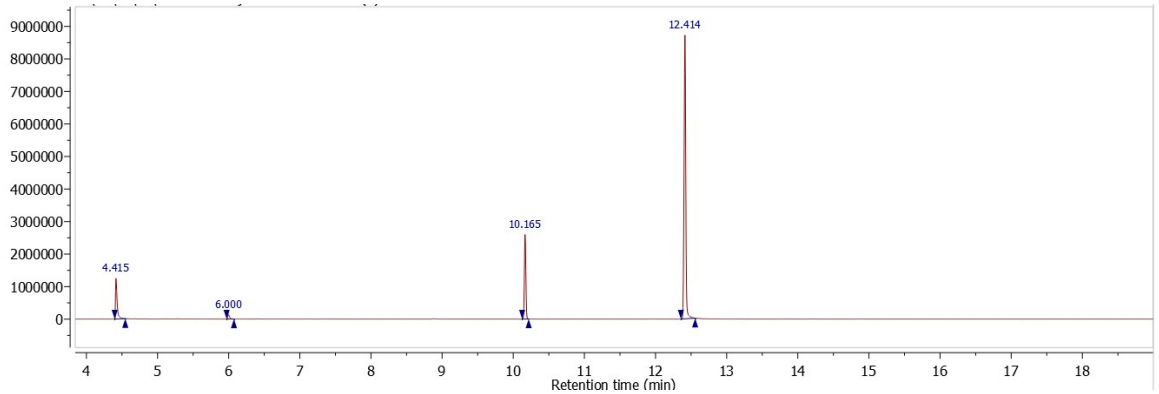

Catalyzed by Al-MIL-53-NH-RNH_2

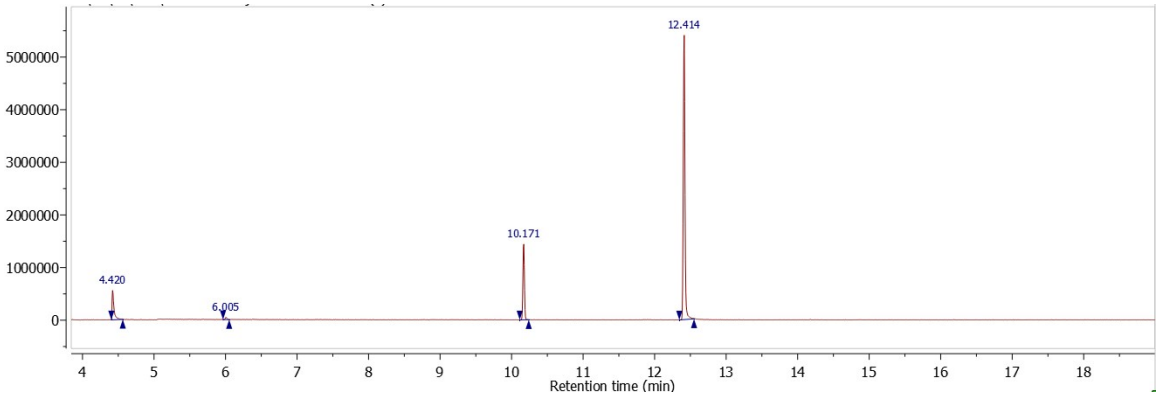

Catalyzed by Cr-MIL-101-NH-RNH_2

Table 4, Entry 1.

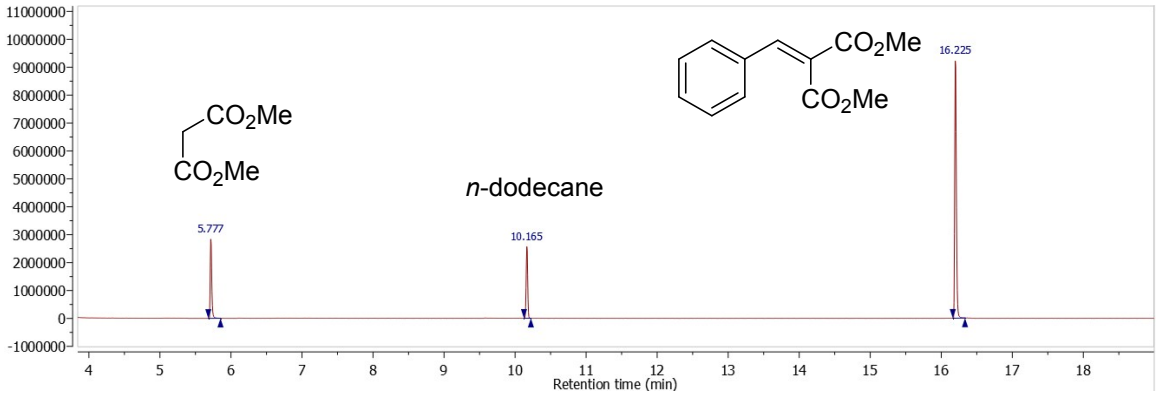

Catalyzed by UiO-66-NH-RNH_2

Table 4, Entry 2.

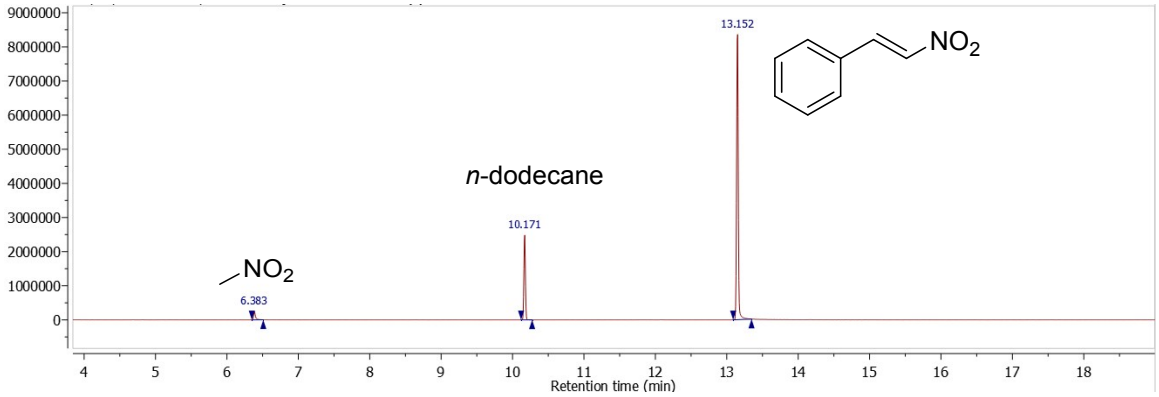

Catalyzed by UiO-66-NH-RNH_2